I. PLASMA PHYSICS OF ELECTRIC ROCKETS

George R. Seikel, Denis J. Connolly, Charles J. Michels, Edward A. Richley, J. Marlin Smith, and Ronald J. Sovie

Most electric thrusters make use of plasma. This paper attempts to focus on the major plasma processes of two basically different type thrusters, which are being investigated over a wide range of power levels (figs. I-1 and I-2). They are the electron bombardment ion thruster and the magnetoplasmadynamic (MPD) arc thruster. Discussions of alternative types of electric thrusters are included in references 1 to 4.

NASA Lewis Research Center has been doing research on both electron bombardment ion thrusters and MPD arc thrusters for a number of years. In both, a plasma is created by a dc discharge between a central cathode and a cylindrical anode in a diverging axial magnetic field, and ultimately a high velocity plasma exhaust is produced.

The ion and arc thrusters, however, employ completely different concepts to accelerate the propellant. The ion thrusters use strong electric fields applied by an accelerator grid to extract and accelerate the propellant ions produced in the discharge. The MPD arc thruster uses forces produced by the interaction of currents and magnetic fields to accelerate the plasma.

This paper will mention the current status and performance of both of these thrusters. But, the approach will be to primarily examine how they work and what limits their performance. The major inefficiencies in both are shown to result from the same plasma processes.

ELECTRON BOMBARDMENT ION THRUSTER

Concept

The electron bombardment thruster is a member of a broader family of thrusters known as electrostatic thrusters. These thrusters differ mainly in the manner in which they create ions. They are basically the same in terms of the method of accelerating the ions and it is from that process that they get their name. Fig-

ure I-3 illustrates the electrostatic acceleration process. An ion source is shown followed by an accelerator electrode system. An electric field is established between the set of electrodes in such a manner that it causes, in this case, positively charged ions to be accelerated to the right and leave the spacecraft. For each ion that leaves the spacecraft, though, an electron remains that must be removed so that the spacecraft will maintain charge neutrality. These electrons are shown being introduced into the beam downstream of the thruster. The lower portion of the figure shows a potential field diagram of the potentials as they would exist in the electrode system and downstream of the thruster. Thrust per unit area is proportional to the square of the field strength, which is labeled E_a in the figure. At Lewis we have worked mainly with electron bombardment thrusters. This thruster was invented by Harold Kaufman, a research scientist at Lewis (ref. 5).

Bombardment Thruster Configuration

Figure I-4 is a schematic diagram of a 15-centimeter-diameter SERT II thruster (SERT stands for Space Electric Rocket Test). In 1964, Lewis managed the SERT I flight test. This test was a ballistic flight launched from Wallops Island which served to demonstrate that electron bombardment thrusters would work in space. Lewis is presently preparing for the SERT II flight test which will be a 6-month duration test of an electron bombardment thruster.

This SERT II thruster operates as follows. Liquid mercury propellant is brought in from the left and contacts the vaporizer which is a heated porous plug. There it is vaporized and the mercury vapor passes to the right into a plenum chamber where it then passes (see the small arrows in the fig. I-4) into the main body or discharge chamber. A small portion of the propellant enters the discharge chamber through the hollow cathode. In the chamber a mercury plasma is created as a result of electrons which are emitted from the hollow cathode and keeper arrangement. The electrons pass into the chamber, ionize the propellant, and eventually arrive at the anode. The entire chamber including the screen electrode is maintained at high positive potential. The accelerator electrode is maintained at a negative potential and an appropriate electric field is established between these two electrodes so that ions from the discharge are extracted, accelerated, and exhausted to the right. The neutralizer cathode and keeper arrangement is used to introduce electrons into the exhaust beam. The thruster is surrounded by a grounded screen that would be maintained at spacecraft potential. To enhance the ionization process, a weak magnetic field is imposed on the discharge chamber by means of bar magnets located around the periphery of the chamber and which are in contact with soft iron pole pieces. As

illustrated in figure I-5, magnetic flux emanates from the tips of the so-called pole pieces and gives rise to a divergent magnetic field in the discharge chamber.

Bombardment Thruster Performance

Bombardment thrusters have been tested at Lewis in sizes ranging from a few centimeters to 150 centimeters in diameter at power levels ranging from a few watts up to 150 kilowatts and at thrust levels ranging from a fraction of a millipound up to 1/2 pound. Figure I-6 summarizes present day performance in terms of the variation in overall efficiency as a function of specific impulse. As a point of reference, the SERT II performance point is shown at about 4500 seconds specific impulse and about 72-percent overall efficiency. The SERT II thruster has been tested in vacuum facilities for more than 3000 hours. Current research is concentrating on the specific impulse range of 2000 to 3000 seconds where, as a result of some recent improvements in thruster performance, efficiencies in the range of 50 to 60 percent are being obtained. This range of specific impulse has been shown from mission analysis studies to be one of great interest for a number of possible applications for electron bombardment thrusters.

For our research investigations, table I-1 shows a summary of a typical thruster performance point for a 30-centimeter-diameter research thruster. From this table it can be seen that the discharge chamber power is a significant portion of the total power and one which we would like to minimize. If the discharge chamber power is divided by the beam current, in this case $1\frac{1}{2}$ amperes, the resulting parameter is the amount of energy required to create an ion in the beam. This parameter is called "eV per ion" and is used to evaluate the effects of various thruster modifications. This parameter is plotted in a number of different ways. For example, figure I-7 is a plot of the discharge energy against propellant utilization efficiency. The propellant utilization efficiency is the beam current divided by the flow into the thruster expressed as an equivalent current. Here we see that the eV per ion stays at about 200 up to a value of utilization efficiency of about 80 percent. It is interesting to note that when Lewis started research on the electron bombardment thrusters (about 10 years ago) values of eV per ion at 80 percent propellant utilization efficiency were about 1250. So there has been more than a factor of six improvement over this 10-year time period. This improvement has been primarily the result of experimental efforts in the laboratory rather than the development of theories that predict the behavior of the plasma in the discharge chamber. The empirical approach was followed because the plasma of the discharge chamber is very complex as is illustrated by figure I-8.

In figure I-8, the discharge energy loss is plotted against magnetic field strength where, for the purposes of these investigations, the permanent magnets of the thruster are replaced by electromagnets so that the magnetic field can be varied. According to a classical electron diffusion theory, the eV per ion should drop as the magnetic field increases. This is found to be the case in practice up to a point (labeled $B_{critical}$ in this plot). Beyond this magnetic field value it is found that the eV per ion does not decrease in accordance with classical diffusion considerations but in fact may increase and exhibit an anomalous behavior. We have investigated a number of magnetic field configurations to determine their effect on performance. In one case, for example, a magnetic field was configured to be similar to the "minimum B" configurations used in some fusion experimental research programs. This configuration was found to be effective in moving the critical magnetic field value to the right somewhat (fig. I-8) and in suppressing plasma noise in the exhaust beam; however, it was not particularly effective in reducing the eV per ion. Another approach was to use the previously described diverging magnetic field (fig. I-5). This configuration was found to be the most effective in reducing the eV per ion.

Ion Extraction System

The greatest reductions in discharge chamber power, however, have been associated with modifications of the ion extraction system. At Lewis, analog and computer techniques for investigating various ion extraction designs have been developed. For example, figure I-9 shows a single hole of the SERT II grid system as it would be set up for modeling on the digital computer program. On the left the shaded portion represents the plasma of the discharge chamber, and the sheath is shown as the parting line between the plasma and the accelerating field region of the grid system. The screen electrode is depicted by the small rectangular blocks and the accelerator electrode by the larger ones. These blocks represent the web of the grids. With this model the digital computer program yields the ion trajectories as they leave the plasma sheath and pass through the grid system as well as the distribution of equipotentials in the grid region.

One startling improvement in performance associated with the grid system resulted from increasing the screen electrode percent open area. In the past the screen electrode holes were similar in size to the accelerator electrode holes (about a 50-percent open area). It was found that increasing the screen electrode percent open area to about 70 percent reduced the discharge chamber losses by a factor of two. We believe this is primarily a result of exposing more of the plasma sheath

area to the extraction field of the grid system. We have been pursuing approaches which we believe can take further advantage of this idea.

Figure I-10 is a comparison of the conventional grid system just described with a newer one - a glass-coated or composite grid. In the new approach a coating of glass is bonded to the accelerator grid. We believe the plasma attaches to the upstream surface of this glass in such a way that an electric field is established along the surface of the glass. Thus, ions are extracted in much the same manner as with the conventional system. With this newer glass-coated grid, high performance at low specific impulses has been achieved. For example, at 2000 seconds specific impulse values of eV per ion of 200 have been obtained with the glass-coated grid as compared with values of 400 or greater with the conventional grids. Of course, the structural advantages of the single glass-coated grid concept are apparent. It eliminates both the need to maintain close spacing between the screen and accelerator grid and alinement between the screen and accelerator grid. These are two important advantages of this new very attractive grid concept.

Present Research Aims

In summary, electron bombardment thrusters appear to have good efficiency at the higher specific impulse levels, and they recently have been making strong gains in performance in the lower specific impulse regions. In our research programs we are focusing on this lower specific impulse region because of its potential application to a number of missions. Work with the coated optics is continuing, and we are now beginning to examine the possibility of coating other components of the thruster which we believe may result in better performance. Of course, we still need a better understanding of the discharge chamber plasma, and in that respect we have recently initiated a spectrographic experiment which we hope will shed some light on the plasma characteristics.

ION SOURCE POWER BALANCE

As discussed in the preceding section, the major inefficiency in a bombardment ion thruster is the plasma discharge energy expended per beam ion produced. This eV per ion is a gross parameter that characterizes the performance of the ion source. An understanding of the plasma processes that limit a dc ion source performance can be obtained by examining a power balance.

If only unavoidable discharge losses are considered, then the limiting per-

formance can be determined. The two major unavoidable losses in a dc discharge are the power lost to the anode and the power consumed in ionization.

The average electron arriving at the anode brings with it at least twice its kinetic temperature kT_e. It also deposits in the anode the energy it gains falling through the anode work function Φ_A. Since the electron current to the anode will be greater than or approximately equal to the total anode current I_A, the power lost to the anode P_A can be written

$$P_A \gtrsim \left(2 \frac{kT_e}{e} + \Phi_A \right) I_A \tag{1}$$

The discharge power consumed in ionization P_I is

$$P_I \gtrsim I_B \Phi_{EFF} \tag{2}$$

where I_B is the beam ion current and Φ_{EFF} the energy required to produce an ion in the plasma discharge. The greater than sign results from the fact that only in the most advantageous limit would all the ions produced in the discharge be usefully exhausted as beam current.

Volume Ion Production Cost

The volume ion production cost Φ_{EFF} has been evaluated for the sustained tenuous plasmas generated in low pressure discharges by considering the collisional and radiative losses in the plasma volume. Results have been obtained for specific gases (refs. 6 to 8) and an approximate general theory (ref. 9) has also been developed that is applicable to all gases. Jack Dugan discusses the atomic models used in this general calculation in his presentation Plasma Chemistry and Ion-Molecule Interactions. Typical results for the volume ion production cost for mercury are shown in figure I-11. The volume ion production cost in eV per ion is presented as a function of electron kinetic temperature in this figure. The number of ions produced per unit volume can also be predicted as a function of electron kinetic temperature. Of course, the product of the ion production rate and volume ion production cost is the power consumed in ionization and excitation processes per unit volume.

Limiting Ion Source Performance

If only the minimum anode power and ionization power losses are considered, then the limiting performance of a dc ion source can be evaluated. The analysis uses only conservation of energy and current. If the discharge has a constant electron kinetic temperature kT_e (eV), then for a given propellant, discharge voltage V, and anode work function Φ_A, the discharge energy per beam ion is only a function of electron temperature:

$$\text{Energy per beam ion (eV/ion)} = \frac{2\frac{kT_e}{e} + \Phi_A + \Phi_{EFF}}{1 - \frac{2\frac{kT_e}{e} + \Phi_A}{V}} \tag{3}$$

Results for mercury are shown in figure I-12 for $\Phi_A = 4.5$ volts, which is the value for tungsten. The eV per ion curves are shown as a function of kT_e for V = 25, 36, and 150 volts. For each V there is an optimum kT_e. Their locus is shown by the dashed curve.

The eV per ion becomes large at low temperatures because as shown in figure I-11 the volume ion production cost is becoming unbounded. The eV per ion also becomes unbounded as

$$\frac{kT_e}{e} \to \frac{1}{2}(V - \Phi_A)$$

because at this temperature all the power is being lost to the anode. When the discharge is operating near the optimum temperature, approximately half the discharge power is lost to the anode and the outer half is consumed in the inelastic atomic processes in the plasma volume.

These minimum values of eV per ion indicate that the performance of present ion sources (under 200 eV/ion at 36 V) may be approaching a fundamental limit. Such a conclusion is however not warranted since a number of simplifying assumptions have been made in evaluating this power balance. Thus these values should be viewed only as a first approximation to the performance limit of such sources.

These results, however, do demonstrate both the importance of examining the power balances for ion sources, and they do indicate the potential performance gains

possible through raising the discharge voltage. Also, similar calculations for propellants other than mercury showed that cesium and possibly xenon ion thrusters might outperform mercury thrusters at least from the point of view of an energy efficiency.

MPD ARC CONCEPT

A typical MPD arc thruster is shown schematically in figure I-13. Its major components are a cathode, anode, insulator, and magnet. Although MPD arc thrusters are not as highly developed and have not achieved as high a performance as the electron bombardment ion thrusters, they do possess a number of relative advantages. The MPD thrusters are physically and electrically simpler, they have an order of magnitude higher thrust density, and a given thruster can operate over a wide range of specific impulse. An MPD arc thruster system may potentially, also, be substantially lighter than an equivalent ion thruster system.

NASA-Lewis has tested steady-state radiation cooled MPD thrusters at power levels from 100 watts to 40 kilowatts. In the higher power radiation cooled thrusters the magnet must be located as shown in figure I-13 upstream of the anode because of the high heat flux from the radiation cooled anode. If adequate insulation is provided, a permanent magnetic can be used. In the lower power devices one has the option of using a magnet coil surrounding the anode or a combination of both. Water cooled dc MPD arcs have been operated to power levels of over 200 kilowatts and we are also operating a pulsed MPD arc of this same geometry at powers up to 4 megawatts for a fraction of a millisecond.

In the particular category of MPD arc thrusters on which we have been doing research, most of the thrust results from the interaction of an induced azimuthal current and the radial component of the applied diverging magnetic field, the magnetic nozzle. There are, however, also simultaneously present two other thrust mechanisms.

But before discussing the various acceleration mechanisms in an MPD arc, it would be well to examine briefly the general interactions of currents and magnetic fields and electric fields associated with these in a plasma.

Plasma Ohm's Law

Figure I-14 shows a vector diagram of plasma current, magnetic field, and electric field. The figure illustrates first that if you pass a current through a

plasma or any other conductor in the presence of a magnetic field you get a Lorentz force or electromagnetic force, which is the vector product $\vec{j} \times \vec{B}$ and is perpendicular to both the current density $\vec{j}$ and the magnetic field $\vec{B}$. In a plasma you get some other effects that are not so common in ordinary conductors. The electric fields that are associated with this current are comprised of the normal resistive component j/σ that is parallel to the current (σ being the conductivity) plus a component of electric field perpendicular to the current flow direction. This is termed the Hall field, and it is given by the quantity $(\omega\tau/\sigma)\left[\left(\vec{j}\times\vec{B}\right)/B\right]$. The parameter $\omega\tau$ is defined as the electron Hall parameter where ω is the electron cyclotron frequency (i.e., the frequency with which electrons spin around the magnetic field lines), and τ is the mean time for an electron to lose its momentum by collision. As a result, the equivalent electric field E^* in figure I-14 is comprised of two components and is not parallel to the current. The angle between the equivalent electric field and current is denoted here as θ. The arc tangent of θ is equal to the Hall parameter times the sine of the angle between the magnetic field and the current:

$$\tan^{-1}\theta = \omega\tau \sin\varphi$$

The corresponding Ohm's law is

$$\vec{E}^* = \frac{1}{\sigma}\left[\vec{j} + \omega\tau\left(\frac{\vec{j}\times\vec{B}}{B}\right)\right] \tag{4}$$

where the equivalent electric field is defined

$$\vec{E}^* = \vec{E} + \vec{v}\times\vec{B} + \frac{\nabla p_e}{en_e} \tag{5}$$

which is the sum of the applied field plus a $\vec{v}\times\vec{B}$ field plus a term due to the electron pressure gradient divided by the electron charge density.

Instabilities and Turbulence

In addition to the Hall effect on Ohm's law there are effects due to oscillations or turbulence. Since plasmas are rarely quiescent, oscillations are nearly always present. In some cases these fluctuations are of sufficiently small amplitude that

they can be ignored. However, under some circumstances (generally termed instability) these oscillations grow to such large amplitudes that they totally govern the phenomena being observed. Here are some examples of these circumstances:

First is the anomalous or Bohm diffusion - that is, the enhanced diffusion of charged particles across magnetic field lines. This diffusion is important in the nuclear fusion field since here the endeavor is to contain charged particles within magnetic field configurations. This is discussed in greater detail in the paper by Rayle et al. As already mentioned, anomalous diffusion also is the cause of an increased energy to produce an electron-ion pair in the ion thruster and hence leads to a decrease in the efficiency of the device.

Second, fluctuations also play an important role in the performance of MHD power generators as is discussed in the paper by Lester Nichols. In this case fluctuations lead to a saturation of the Hall parameter at a value of the order of one even though the magnetic field is continually increased. This is an undesirable result since the performance of these devices is a strongly increasing function of the effective Hall parameter.

Third, in MPD accelerators the phenomenon appears to manifest itself by concentrating the current in the form of a rotating current spoke rather than allowing it to have azimuthal symmetry about the cathode.

To illustrate the influence of oscillations on plasma devices, consider their effect on Ohm's law. From a theoretical standpoint, the problem is one of providing a theory which agrees with what is observed experimentally. This can best be understood by recognizing that while Ohm's law as presented (eq. (4)) may well be valid within the little black box which is the experiment, we are in general observing that experiment from the outside by way of ammeters and voltmeters which cannot resolve in time or space the high frequency oscillations in the plasma. So in effect average values are measured. Therefore, the theory need only predict these average values.

To better understand this statement, consider the effect of electron density fluctuations on Ohm's law. For simplicity assume the following: (1) the pressure gradients are negligible, (2) only Coulomb collisions are important so that the electrical conductivity σ is independent of the electron density, and (3) the induced magnetic field is negligible relative to the constant applied external field so that the cyclotron frequency ω and the magnetic field $\vec{B}$ are also independent of time. Therefore, σ, ω, and B are independent of time as denoted by the subscript o.

It is convenient for theoretical development to separate the current into two parts:

$$\vec{j} = \vec{j}_o + \vec{\tilde{j}} \tag{6}$$

so that the measured or average value is

$$\langle \vec{j} \rangle = \vec{j}_o \tag{7}$$

Therefore in order to obtain correspondence between theory and experiment an expression must be established for $\vec{j}_o$. To do this, the quantities $\vec{j}$, $\vec{E}$, and τ are written as in equation (6) (i.e., the sum of an average plus fluctuating part) and substituted into Ohm's law (eq. (4)) which is then averaged to yield

$$E_o = \frac{1}{\sigma_o}\left(\vec{j}_o + \omega_o \tau_o \frac{\vec{j}_o \times \vec{B}_o}{B_o} + \omega_o \tau_o \left\langle \frac{\tilde{n}_e}{n_{eo}} \tilde{\vec{j}} \right\rangle \times \frac{\vec{B}_o}{B_o} \right) \tag{8}$$

where we have used the fact that τ is inversely proportional to n_e for Coulomb collisions and have assumed that the fluctuation quantities are sufficiently small so that we need only retain terms which are quadratics - that is, to order of the product of fluctuating quantities.

Equation (8) has the same form as equation (4) except it contains the extra term $\omega_o \tau_o \langle (\tilde{n}_e/n_{eo}) \tilde{\vec{j}} \rangle \times (\vec{B}_o/B_o)$ which can be put in a more conventional form by multiplying equation (4) by $\tilde{n}_e/n_{eo}$ and again averaging using the additional relations $\nabla \times \vec{E} = 0$ and $\nabla \cdot \vec{j} = 0$ to obtain

$$\vec{E}_o = \frac{1}{\sigma_{EFF}} \left[\vec{j}_o + (\omega\tau)_{EFF} \frac{\vec{j}_o \times \vec{B}_o}{B_o} \right] \tag{9}$$

which has exactly the same form as the original Ohm's law but σ and $\omega\tau$ are effective values given by

$$\sigma_{EFF} = \frac{\sigma_o}{1 + \left\langle \frac{\tilde{n}_e^2}{n_{eo}^2} \right\rangle (\omega_o \tau_o)^2} \tag{10}$$

$$(\omega\tau)_{EFF} = \frac{\omega_o \tau_o}{1 + \left\langle \frac{\tilde{n}_e^2}{n_{eo}} \right\rangle (\omega_o \tau_o)^2} \tag{11}$$

Obviously transport coefficients are grossly modified from their steady state or usual gas kinetic values (i.e., τ_o and $\omega_o\tau_o$) in the presence of fluctuations as $\omega_o\tau_o$ becomes large.

In order to establish the magnitude of the fluctuation $\left\langle n_e^2/n_{eo}^2 \right\rangle$, one must evaluate in the presence of the electron density fluctuation all other pertinent equations (i.e., electron density, etc.). In the case of MHD generators, for example, it can be shown (ref. 10) that

$$\left\langle \frac{\tilde{n}_e^2}{n_{eo}^2} \right\rangle \propto \frac{1}{\omega_o\tau_o}$$

so that $(\omega\tau)_{EFF} \to$ constant as $\omega_o\tau_o \to \infty$; that is, the effective Hall parameter saturates.

Later in this discussion results are presented of some calculations performed in the supersonic expansion region of a MPD thruster where reasonable agreement with experiment is obtained assumming $(\omega\tau)_{EFF}$ = constant.

MPD Acceleration Mechanisms

Figure I-15 illustrates the current and magnet field distribution in a typical MPD arc thruster. Current is shown with solid lines and magnetic field by dashed lines. The applied arc current between the anode and cathode flows radially with some pluming into the exhaust. The applied magnetic field diverges to form what can be termed a magnetic nozzle. In addition to the applied magnetic field there is an azimuthal magnetic field which is caused by the applied arc current itself. In addition to the applied arc current there is, as already indicated, an induced azimuthal current. Why it is there will be explained shortly.

With this geometry and these currents and fields there are three basically different thrust mechanisms simultaneously present:

1. Pressure on the physical nozzle
2. Direct magnetic pumping, $j_r B_\theta$
3. Magnetic nozzle processes, $j_\theta B_r$
   - (a) Expansion
     - (1) Recovery of thermal energy, $j_\theta \propto \partial p/\partial r$
     - (2) Recovery of swirl energy, $v_\theta \propto j_r B_z$
   - (b) Drift current, $j_\theta \propto \vec{E} \times \vec{B}$

The first is simply the ordinary gas dynamic pressure on the physical anode nozzle. The second is the direct plasma acceleration which is termed magnetic pumping (sometimes also termed blowing) and is the result of the interaction of the radial current and the azimuthal magnetic field. The third category is the magnetic nozzle plasma acceleration process which results from the interaction of the azimuthal current with the radial field of the magnetic nozzle.

As indicated, there are two major subcategories of magnetic nozzle processes. The first subcategory, the processes termed "expansion" in a magnetic nozzle, is analogous to expansion processes in an ordinary physical nozzle. In the conversion of thermal energy into directed energy in a magnetic nozzle, the radial plasma pressure gradient gives rise to a diamagnetic azimuthal current. With regard to the second subcategory of expansion processes, the interaction of the applied arc current and applied magnetic field causes rotational or swirl energy to be added to the plasma. In the subsequent expansion in the magnetic nozzle, energy and angular momentum are conserved, and the swirl energy is converted into directed energy. Associated with this conversion is an azimuthal current driven by the $\vec{v} \times \vec{B}$ electric field. Thus associated with expansion processes in a magnetic nozzle are two mechanisms that cause azimuthal current to be induced in the magnetic nozzle. A third alternative mechanism is the drift current which may result from the interaction of the applied electric and magnetic fields.

For any given MPD arc experiment the thruster mass flow, current, and magnetic field can be adjusted so as to make any one of the mechanisms discussed important. Conversely, to determine how a given MPD arc thruster is producing thrust requires an assessment of the relative importance of the various possible thrust mechanisms. As indicated earlier, research at Lewis has been aimed at attempting to utilize primarily the magnetic nozzle thrust mechanisms. One can then view the magnetic nozzle MPD arc thrusters as an arc jet in which the physical nozzle has been replaced by a magnetic nozzle so that the gas dynamic heat-transfer losses of the physical nozzle are avoided.

MPD ARC THRUSTERS

NASA-Lewis is investigating MPD thrusters at both the subkilowatt and multikilowatt power levels. Figures I-2 and I-16 are cutaway drawings of the 30- and 1/2-kilowatt thrusters. Both operate on low voltage dc and have radiation cooled anodes. The two thrusters differ in mass flow rate, power, and thrust level, but have comparable size, efficiency, and specific impulse.

The multikilowatt MPD thruster (fig. I-2) operates with an arc power near 30 kilowatts and produces thrust of about 1/2 newton (1/10 lb). Generally NH_3 is used as propellant. Ionization of the plasma exhaust of this thruster is between about 10 and 100 percent. The thrust is developed primarily through magnetic nozzle effects since data show that most of the ion acceleration occurs out in the magnetic nozzle. The ions also apparently drag many neutral particles along with them. Some thrust, of course, is also due to gas-dynamic effects.

The 1/2-kilowatt MPD thruster shown in figure I-16 operates with an arc power of a few hundred watts. The thrust produced is a few millipounds. Xenon propellant has yielded the highest efficiency. It has a lower density discharge that ionizes almost all the propellant atoms. The acceleration in this case also takes place out in the magnetic nozzle.

Subkilowatt MPD Arc Thruster

In addition to performance measurements, the earliest work done on the subkilowatt thruster was to determine the dominant acceleration mechanism. Figure I-17 shows schematic views of the subkilowatt thruster and profiles of the plasma potential and electron pressure measured by Bowditch (ref. 11). The plasma potential profiles were obtained by emissive probes and the magnetic field lines by magnetic field probes. Generally the electric field is parallel to the magnetic field. This shows no serious currents can arise caused by $\vec{E} \times \vec{B}$ drifts. The potential profiles show that the accelerator voltage drops associated with ion acceleration occur out in the magnetic nozzle.

The electron pressure profiles were obtained by using a Langmuir probe to obtain the electron number density and electron temperature from which the electron pressure was calculated. The gradient of electron pressure divided by the electron density along the axis is found to be proportional to the electric field in that direction. This says that the acceleration occurs in a space-charge free region supported by the electron pressure gradient (refs. 11 and 12).

If the electron pressure is integrated over the area of the station shown at the edge of the nozzle, the resultant force approximates the measured thrust, thus further supporting this magnetic nozzle model. The ions get their energy at the expense of the random electron energy. The ions and electrons are tightly coupled by the requirement that no net currents leave the thruster. Since this was anticipated to be the dominant acceleration mechanism, earlier versions of low power MPD arc thrusters were termed magnetic-expansion thrusters (similar devices have also been

termed oscillating electron thrusters or nonequilibrium magnetically contained electrothermal thrusters).

Other diagnostic work done on this thruster has included determining (ref. 13) that most of the accelerator voltage drop occurs near the cathode. Hence, arc impedance can be controlled by varying the hollow cathode flow. This flow is a few percent of the total propellant flow.

Magnetic Expansion Process

Walker and Seikel have examined analytically the type expansion process found in the low power MPD arc thruster. Specifically, the expansion of a fully ionized plasma containing hot electrons and cold ions is examined in the magnetic nozzle produced by a Helmholtz set of coils (fig. I-18). The analysis is restricted to near the axis of symmetry and the effects of thermal conduction are included since, as will be shown, these can be important.

The set of equations to be solved includes the electron and ion continuity and momentum equations, Maxwell's equations, and an electron energy equation. No asymptotic solutions to this nonlinear set of equations for large values of z were found using classical values of the conductivity for the plasma. As a result and due to the fact that in the experiments major fluctuations were present, an assumption was introduced that the electron collision time could be replaced by an effective time in the manner described in the earlier fluctuation discussion. In particular, the assumption was made that the effective Hall parameter be a constant throughout the flow. Such an assumption assumes a saturation of this parameter of the type previously described as being appropriate at least for MHD generators.

With this additional assumption, the solutions to the plasma expansion shown in figure I-19 were obtained. The ordinate is the ratio of the final ion energy to the initial electron energy - that is, the final ion energy at the end of the expansion divided by the random energy the electrons had back before the expansion started. This is plotted against the sonic point location. The sonic point location is relative to the downstream coil in the Helmholtz set: zero is at the plane of the coil, and the location is given in coil radii. The parameter in the analysis is a nondimensional parameter best though of as a nondimensional magnetic field.

These solutions illustrate a couple of points. First, the magnitude of the ratio of the final ion energy to the initial electron energy can be much larger than what you would get in an adiabatic expansion. The adiabatic expansion result is shown by the dotted line, and this illustrates how important the thermal conduction can be in such a process. The second point is that for sonic point locations near the plane of the

downstream coil the solutions are fairly insensitive to the sonic point location. However, if the sonic point moves a coil radii downstream of that plane, then the solutions become very sensitive to the sonic point location.

The results of this analysis can be used to make a power balance for the low power MPD arc thruster. The results of figure I-19 give the final energy of the ion in terms of the upstream temperature. As described earlier, in making a power balance for the ion sources, the anode losses for such a discharge are also a function of the upstream electron temperature as are the ionization losses. Thus, the results of figure I-19 can be combined with the minimum anode power and volume ionization power losses to make a power balance for the low power thruster. This results in predicting a limit to the efficiency as a function of specific impulse. The results of such a calculation are shown in the figure I-20. Calculations were done for xenon propellant, a discharge voltage of 100 volts, and an anode work function of 4.2 volts corresponding to molybdenum. To make these calculations the sonic point location was assumed to be at the plane of the downstream coil. Corresponding to every point along this theoretical limit curve of figure I-20 is an optimum discharge electron temperature and optimum nondimensional magnetic field.

Figure I-20 also shows the efficiency as a function of specific impulse of the present NASA-Lewis low power xenon MPD arc thrusters (ref. 8). The discrepancy between the experiments and the theoretical limit may indicate some substantial gains are possible in the experimental performance of such thrusters. Caution should be exercised though since to make these theoretical limit calculations required assuming the sonic point location. If the sonic point were actually much further downstream than the plane of the downstream coil, then the theoretical limit would be lower. This point brings up one of the big problems yet to be answered for such flows: Where does the sonic point occur and why?

This expansion process that has been described relative to the low power thruster is also present in the higher power devices. But for the high power devices a number of additional effects must be included; for example, it can be shown that the ion temperature must be included. The higher power devices are also only partially ionized. Some of the effects of swirl and pluming of current down into the nozzle may also have to be included. As a result, not much work has been done on the supersonic expansion for the high power thruster; there has, however, been some analytical work done upstream of the sonic point for these higher power devices.

High Power MPD Subsonic Theory

Typical of the high power MPD arc thruster subsonic analyses is the work of

Workman (ref. 14). Basically, he considers the device to consist of two concentric electrodes with constant flow area upstream of the throat and a downstream diverging expansion region. He then considers the flow of a multicomponent chemically reacting fluid through a constant area duct with heat addition to drive the fluid sonic at the throat. As was pointed out in the preceding section and also by Seals and Hassan (ref. 15), one does not necessarily have to have the sonic point at the throat of the device since the Ohmic heating may extend downstream of the throat allowing the sonic point to occur in the downstream expansion region. The interesting point of Workman's analysis is the fact that the current tends to concentrate at the throat in a distance which is of the order of millimeters while typically the dimensions of these throats are of the order of centimeters. In other words, the current tends to concentrate in a sheet. This current sheet is also observed in the analysis of Rosciszewski (ref. 16).

There is at least some qualitative experimental justification for this result on the basis of the experiments of Shih (ref. 17) as shown in figure I-21. In these experiments Shih segments the anode in the gas flow direction to measure the anode current and heat flux distribution. The anode current distribution is shown by the solid curve. The electric current is very highly peaked in the throat of the device. Therefore, the current attaches over a short distance at the throat.

High Power MHD Exhaust

Although the theory for the supersonic region of the high power MPD arc thruster is not well understood, some interesting diagnostic studies have been made of the plasma exhaust. One such study is to measure the axial velocity of each species in the plasma exhaust and to determine how they vary as the engine operating parameters are changed (refs. 18 and 19). The velocities were obtained by measuring the Doppler shifts of spectral lines emitted by the various plasma constituents.

Some typical results for the MPD arc operating on ammonia propellant are shown in figure I-22. Here the axial velocity of some plasma species is plotted as a function of axial distance from the anode exit plane. These data illustrate facts that were found to be true for all cases studied. The observed ion and neutral velocities always increased substantially in the magnetic nozzle region outside the thruster. The N^{+} and N^{++} ions always reached about the same peak velocity, and this velocity was always greater than that corresponding to the measured specific impulse. Fast neutrals were observed in every run and their velocities approached those corresponding to the measured specific impulse.

The variation of ion and neutral velocities was studied for a variety of operating

conditions. Consider the trends shown in figure I-23. The data show that increasing the arc power at constant mass flow rate results in higher specific impulse and thruster efficiency. In this case, the better performance is essentially due to an increase in the efficiency of converting the power that is put into the plasma into thrust. Both the ion and neutral velocities increase with increasing arc power. Other measurements also indicate that the degree of ionization and electron temperature increase with arc power in this case.

At constant specific impulse, figure I-23 shows that the efficiency increases with increasing mass flow rate. In this case the exhaust velocities do not change appreciably and it was found that the increased efficiency was due to a decrease in the anode heat loss.

High Power MPD Losses

For the high power MPD arc thrusters the anode losses run from about 45 to 60 percent of the input power depending on mass flow rate, magnetic field, and arc current. The reason for the losses can be illustrated by returning to figure I-21. The dashed curve is the heat flux to the anode surface as a function of axial position along the anode. The solid curve is the current flux. Note that the two curves almost coincide.

This would seem to indicate that almost all of the anode power loss is carried by electrons in the arc current. Simple sheath considerations mentioned before require the anode heat loss per electron to be at least two times the electron temperature plus the anode surface work function. Upper limits on arc electron temperatures estimated using this rule vary from 10 to 15 electron volts. Such values are at least in qualitative agreement with the previously discussed one-dimensional subsonic high-power MPD theory.

The anode power loss also depends on arc voltage mode. At a given arc power, the current (and hence the anode power loss) is lower in the high voltage mode. Voltage mode behavior is closely related to the way current attaches to the cathode. In this connection, figure I-24 shows an interesting sequence of photographs obtained by McDonnell-Douglas. Each shot of figure I-24(b) shows the cathode tip of the radiation cooled thruster of figure I-24(a) viewed through the anode throat at about a 45° angle. The time from the start of the sequence (in hours) and the arc voltage at the time of the photograph are shown alongside each picture. Note incidentally that the photographs were taken more than 500 hours into an endurance test of the radiation cooled thruster. The first case has the highest arc voltage and light emanating primarily from the tip of the cathode. In succeeding cases one sees a

progressive decrease in arc voltage and a progressive trend toward current attachment further back on the cathode. In the last case the voltage has dropped drastically and the current attachment has shifted to the extent that only the tip is dark.

Operating in the low voltage mode shown in this last picture is detrimental to thruster life. It does, however, produce somewhat higher arc efficiency in spite of the higher anode losses. Hence the power that is put into the gas is much more efficiently converted to thrust in the low voltage mode.

The present performance of the 30-kilowatt radiation cooled thruster (fig. I-24(a)) is shown in figure I-25. These data (ref. 20) show both that the efficiency increases with arc power and that at constant power the specific impulse can be varied over a wide range. This thruster was developed by McDonnell-Douglas under contract to NASA-Lewis (ref. 21). It represents the first truly radiation cooled high power MPD arc thruster. The thruster is designed with adequate insulation between the anode and the magnet so that a radiation cooled permanent magnet could be utilized.

We are presently looking into the processes which effect the way current attaches to the cathode. We hope that by learning to control this we can raise the arc voltage to lower anode losses while maintaining the advantage of the low voltage mode current distribution.

Unsteady MPD Arc Phenomena

Thus far only the time average current distribution has been discussed. Its dynamic behavior is more complicated. MPD thrusters operate over a wide range of conditions with the current concentrated into a rotating spoke as depicted in figure I-26. The spoke rotates in the $\vec{j} \times \vec{B}$ direction along with the plasma flow. In the higher power thruster the frequency of rotation is usually from about 100 to 500 kilohertz (ref. 22). The frequency increases with increasing arc current or magnetic field strength and decreases with increasing mass flow rate or anode throat diameter.

In our typical data the current spoke is about one-third of a circle in width. It is very rich in harmonic content. Occasionally low order harmonics are larger than the fundamental. There is a complete absence of a phase difference between otherwise identical measurements made at different axial positions. This indicates that there is no component of propagation in the axial direction. For the low power MPD arc thruster, the same general picture holds but the spoke frequency is lower (10 to 60 kHz, ref. 23). Also present in this thruster is a total arc current ripple or pulsing fluctuation. In these experiments Burkhart also shows that the magnitude

of both the spoke and ripple current fluctuations could be affected by the ac impedance of arc circuit.

At present it is not clear whether the current spoke is detrimental to performance. It does, however, greatly complicate MPD arc theory and experiments to no clear advantage. One approach being considered, therefore, is to look for ways to get rid of it. Preliminary tests with the low-power thruster for example indicate that use of inductors in series with an azimuthally segmented anode will eliminate the current fluctuations on the segments.

Rotating Spoke Theory

Smith (ref. 24) has theoretically studied the formation of MPD arc spokes as the result of instabilities generated by electron density and/or temperature fluctuations in the current sheet region of the device. The theory also predicts pulsations (as have been observed in the low power arcs) as well as rotational instabilities. However, only the purely rotational component has thus far been compared to experimental data. The data used are for the high power thruster experiments of Connolly et al. (ref. 22) and Malliaris (ref. 25). Typical results are shown in figures I-27 and I-28.

Frequency versus mass flow. - The order of magnitude agreement in figure I-27 is good; however, the theoretical curve tends to rise more abruptly than the data with increased current. This behavior may be associated with the breakdown of the fundamental spoke mode into a number of higher harmonics or may indeed result from the destabilization of new fundamental modes. Such nonlinear effects cannot be accounted for by the present linear theory but have (as was noted) been experimentally observed.

Frequency versus mass flow. - The interesting point in figure I-28 is the abrupt rise in frequency as one goes to low mass flows which are both experimentally observed and analytically predicted. This analysis has also found (consistent with experimental observations) that the spoke frequency increases with the magnetic field and decreases with increasing atomic mass of the working fluid.

Another theory based on the formation of spokes as a result of Simon-Hoh type instabilities in the gradient dominated region around the electrodes has been considered by Hassan (ref. 26). He has had some success in predicting the onset conditions measured at NASA-Langley (ref. 27).

PULSED MPD ARCS

In contrast to the spoke characteristics of the steady-state low and high power MPD arc, if MPD arc devices are scaled to very high power levels (0.2 to 5 MW) and operate for less than milliseconds, no spokes are found to exist. These investigations of a pulsed megawatt arc plasma source at Lewis are the outgrowth of the coaxial plasma gun research summarized in reference 28.

Figures I-29 and I-30 show views of this pulsed megawatt MPD arc plasma source. Figure I-29 is a side view of the source, which is about a meter long. On the right is the dewar for the superconducting magnet. The magnet provides fields of from 0 to 2.5 tesla at its center where the arc chamber is.

The source operates for a fraction of a millisecond, sending plasma streaming to the right into an evacuated glassware test section. The arc is powered by a crowbarred capacitor bank and inductor and uses a puff source of gas. The electromagnetic hammer for the fast gas valve is shown on the left, and below it are the cables for the cathode heater.

A better view of the arc chamber is shown in figure I-30. This is an iron fillings map of the magnetic field in the arc chamber area. The anode is a simple copper ring and the cathode is a heated tungsten ribbon. Behind the cathode are the gas ports for the propellant.

The early work on this pulsed source determined that no spokes exist and investigated the voltage-current characteristics of the arc. Since this is a pulsed experiment and since voltage-current curves are sensitive to frequency, it would be well to review for a moment how arc characteristics can change with frequency. Figure I-31 shows the voltage-current curve for a resistor; this curve is linear, positive sloped, and does not change with frequency. Also shown in this figure is the static voltage-current characteristic for a simple, low-current arc. It is curvilinear, negative sloped, and the characteristic varies with frequency. With slow enough current variations the static curve is followed. As frequency increases, the dynamic curves gradually change form and slope until almost resistor-like characteristics occur at high frequency. This is the realm of the Lewis pulsed arc source being investigated.

Although argon and nitrogen have been examined in this source, this discussion is limited to nitrogen (ref. 29). Figure I-32 shows a series of four shots, each with a higher peak current. Each shot has the same mass flow and magnetic field. The last shot shows a peak current of 13 kiloamperes and a peak power of 2.5 megawatts. Each shot represents about 100 microseconds of data, with time progressing toward lesser current values. These are dynamic characteristics taken at various points along the static curve, which lies somewhere in the shaded area. We have arbitrarily

shown the approximate static curve going through the midpoints of the dynamic curves. If the mass flow is held constant but the magnetic field is increased, then the shaded area becomes less negatively sloped. Thus the family of shots provides dynamic as well as approximate static characteristics, which are both important characteristics for the control, powering, and classification of arcs.

Another experiment now in progress employs laser scattering diagnosis in the exhaust 0.50 meter downstream of the device. Preliminary results show the exhaust electron density to be about 10^{20} particles per cubic meter and an electron temperature of a few electron volts. Combining the density measurement with a Faraday cup measurement in that area shows the stream velocity to be 1×10^{4} to 2×10^{4} meters per second. In a future experiment we hope to measure transient pressures, both static and dynamic.

THRUSTER TEST FACILITIES

NASA-Lewis has two large vacuum facilities (ref. 30) for testing electric and electromagnetic thrusters (fig. I-33) and a number of smaller facilities. In these facilities ion thrusters and MPD arc thrusters are tested at sufficiently low background pressures so that the problems of electrical breakdown and background mass entrainment are not present.

Without facilities capable of providing such low background pressures, erroneous performance measurements and beam diagnostics may be obtained. Thus, background pressure effects for MPD arcs were investigated at Lewis (ref. 31). Figure I-34 shows some illustrative results obtained for a MPD thruster running on hydrogen propellant with the background pressure increased by bleeding nitrogen into the vacuum tank. The upper portion of the figure shows how the measured thrust changed as a result of increasing the background pressure. The lower portion shows how the axial velocity of the hydrogen propellant and the product of the velocity and intensity of the background nitrogen ions change with increasing pressure. This latter quantity is used as an indicator of how the background gas entrainment effects change.

As one starts at the normal operating pressure and bleeds nitrogen into the tank, the propellant velocity is unchanged for a while and then begins to decrease. At essentially the same pressure the background nitrogen ion spectrum line intensity and Doppler shift become detectable. As the pressure is further increased the propellant velocity continues to decrease and the background entrainment increases rapidly. The former effect will reduce the measured thrust and the entrainment will increase it. Thus the observed thrust can either increase or decrease depending on

which effect is dominant. Mass entrainment can double the observed thrust at a pressure of around 0.2 torr.

Consequently, the efficiencies reported for thruster studies made in facilities that do not have the pumping speed necessary to supply the proper low pressure environment are somewhat questionable. Furthermore, beam diagnostic studies in these facilities could also be questioned since one could not separate the effects of the primary propellant and background gas.

SUMMARY OF MPD EXPERIMENTS

In summarizing the MPD arc experiments, we might indicate that we have had fair success making measurements of plasma properties out in the beam. Probes can be used to measure electron temperature, number density, and beam power flux. Using spectroscopic Doppler shift techniques yields detailed information on the velocities of the particles in the beam. More complete diagnostic studies using these techniques coupled with extensions to the analysis of the plasma magnetic nozzle expansion discussed herein should lead to an understanding of the acceleration processes.

The interelectrode region, however, is another matter. The energy density is too high for conventional probes to last more than a few hundred milliseconds. The spatial resolution required is too fine for water-cooled probes. Both probe and spectroscopic measurements are greatly complicated by the rotating current spoke, and although some analysis is available, it is clear that much more work is required in this region to obtain a good understanding of device operation.

SUMMARY

To summarize the plasma processes in the electron bombardment ion thruster and MPD arc thruster, we have shown that in both types of thruster the major inefficiencies are the result of the same plasma processes. In both cases these are (1) the fundamental power losses associated with carrying current to an anode, and (2) the loss of power associated with ionizing a plasma.

Fortunately, in the ion thruster the total power expended in the plasma discharge ion source can be kept small compared to the ion acceleration power and high efficiency can be obtained.

In MPD arc thrusters all the power is put into the plasma discharge, and thus the anode losses are a large fraction of the total power. Since the anode power loss

is directly proportional to current, the most obvious method of lowering this loss is to operate the arcs at a higher voltage. We are exploring this approach as well as examining the possibility of lowering the power required for ionization by using only partially ionized plasma propellants.

REFERENCES

1. Jahn, Robert G.: Physics of Electric Propulsion. McGraw-Hill Book Co., Inc., 1968.
2. Mickelsen, William R.; and Kaufman, Harold R.: Status of Electrostatic Thrustors for Space Propulsion. NASA TN D-2172, 1964.
3. Domitz, Stanley; Kosmahl, H. G.; Ramins, Peter; and Stevens, N. John: Survey of Electromagnetic Accelerators for Space Propulsion. NASA TN D-3332, 1966.
4. Wallner, Lewis E.; and Czika, Joseph, Jr.: Arc-Jet Thrustor for Space Propulsion. NASA TN D-2868, 1965.
5. Kaufman, Harold R.: An Ion Rocket with an Electron Bombardment Ion Source. NASA TN D-585, 1961.
6. Sovie, Ronald J.; and Klein, Barry M.: Volume Ion Production in a Tenuous Helium Plasma. NASA TN D-2324, 1964.
7. Sovie, Ronald J.; and Dugan, John V., Jr.: Energy Required for Ion Production by Electron Bombardment in Helium, Argon, and Cesium. Presented at the 17th Annual American Physical Society Gaseous Electronics Conference, Atlantic City, N.J., Oct. 14-16, 1964.
8. Sovie, Ronald J.; and Dugan, John V., Jr.: Effects of Metastable Atoms on Volume Ion Production in a Tenuous Helium Plasma. NASA TN D-3121, 1965.
9. Dugan, John V., Jr.; and Sovie, Ronald J.: Volume Ion Production Costs in Tenuous Plasmas: A General Atom Theory and Detailed Results for Helium, Argon, and Cesium. NASA TN D-4150, 1967.
10. Sobles, Albert: Quasi-Linear Plane Wave Study of Electrothermal Instabilities. Electricity from MHD, Vol. 1. International Atomic Energy Agency, 1968, pp. 499-518.
11. Bowditch, David N.: Investigation of the Discharge and Exhaust Beam of a Small Arc Plasma Thrustor. Paper 66-195, AIAA, Mar. 1966.

12. Seikel, George R.; Bowditch, David N.; and Domitz, Stanley: Application of Magnetic-Expansion Plasma Thrustors to Satellite Station Keeping and Attitude Control Missions. Paper 64-677, AIAA, Aug. 1964.

13. Johansen, A. E.; Bowditch, D. N.; and Burkhart, J. A.: Experimental Performance of a Low-Power MPD Arc Thrustor. Paper 67-50, AIAA, Jan. 1967.

14. Workman, J. B.: Arc Structure in a Magnetic Annular Discharge. AIAA J., vol. 7, no. 3, Mar. 1969, pp. 512-519.

15. Seals, R. K., Jr.; and Hassen, H. A.: Analysis of MPD Arcs with Non-equilibrium Ionization. AIAA J., vol. 6, no. 12, Dec. 1968, pp. 2273-2278.

16. Rosciszewski, J.: Acceleration Process in a MPD Arc Jet. Proceedings of Tenth Symposium on Engineering Aspects of Magnetohydrodynamics, MIT, 1969, pp. 112-116.

17. Shih, K. T.: Anode Current and Heat Flux Distributions in an MPD Engine. Paper 69-244, AIAA, Mar. 1969.

18. Sovie, R. J.; and Connolly, D. J.: Doppler Measurements of the Exhaust Velocities in an MPD Thruster. Bull. Am. Phys. Soc., vol. 13, no. 11, Nov. 1968, p. 1513.

19. Sovie, R. J.; and Connolly, D. J.: A Study of the Axial Velcoties in an Ammonia MPD Thruster. AIAA J., vol. 7, no. 4, Apr. 1969, pp. 723-725.

20. Connolly, Denis J.; and Sovie, Ronald J.: Performance of Radiation Cooled Magnetoplasmadynamic Arc Thrusters. NASA TM X-1908, 1969.

21. Esker, D. W.; Kroutil, J. C.; and Checkley, R. J.: Radiation Cooled MPD Arc Thruster. NASA CR 72557, 1969.

22. Connolly, Denis J.; Sovie, Ronald J.; Michels, Charles J.; and Burkhart, James A.: Low Environmental Pressure MPD Arc Tests. AIAA J., vol. 6, no. 7, July 1968, pp. 1271-1276.

23. Burkhart, James A.: Segmented Anode, CO_2-H_2 Performance and Hollow Cathode Erosion Tests on a Low Power MPD Acr Thruster. Paper 69-242, AIAA, Mar. 1969.

24. Smith, J. Marlin: Electrothermal Instability - An Explanation of the MPD Arc Thruster Rotating Spoke Phenomenon. Paper 69-231, AIAA, Mar. 1969.

25. Malliaris, A. C.: Investigation of Acceleration Mechanisms in MPD Accelerators. Rep. AVSSD-0044-68-CR, Avco Corp. (ARL-68-0078, DDC No. AD-674615), Apr. 1968.

26. Hassan, H. A.; and Thompson, Charles C.: Onset of Instabilities in Coaxial Hall Current Accelerators. Paper 69-230, AIAA, Mar. 1969.

27. Allario, Frank; Jarrett, Olin, Jr.; and Hess, Robert V.: Onset of Rotating Disturbance in the Interelectrode Region and Exhaust Jet of an MPD Arc. Paper 69-232, AIAA, Mar. 1969.

28. Michels, Charles J.: A Resume of Research on Coaxial Plasma Guns Performed at Lewis Research Center. Presented at the Seminar on Coaxial Plasma Guns, Catholic Univ. of Amer. Washington, D.C., May 10, 1968.

29. Michels, Charles J.: Dynamic Current-Voltage Characteristics of a Nitrogen MPD-Arc Plasma Source. Presented at the 1969 Fall Meeting of the Ohio Section of the American Physical Society, Columbus, Ohio, Oct. 12-18, 1969.

30. Finke, Robert C.; Holmes, Arthur D.; and Keller, Thomas A.: Space Environment Facility for Electric Propulsion Systems Research. NASA TN D-2774, 1965.

31. Connolly, D. J.; and Sovie, R. J.: The Effect of Background Pressure and Magnetic Field Shape on MPD Thruster Performance. Paper 69-243, AIAA, Mar. 1969.

BIBLIOGRAPHY

This bibliography comprises publications authored by the members of the NASA Lewis Research Center Staff.

Anon.: Proceedings of the NASA-University Conference on the Science and Technology of Space Exploration. Vols. 1 and 2. NASA SP-11, 1962.

Baldwin, L. V.; and Sandborn, V. A.: Theory and Application of Hot-Wire Calorimeter for Measurement of Ion Beam Power. Paper 1389-60, ARS, Nov. 1960.

Baldwin, Lionel V.; and Sandborn, Virgil A.: Hot-Wire Calorimetery: Theory and Application to Ion Rocket Research. NASA TR R-98, 1961.

Banks, Bruce: Composite Ion Accelerator Grids. Presented at the 3rd Electrochemical Society International Conference on Electron and Ion Beam Science and Technology, Boston, Mass., May 6-9, 1968.

Banks, Bruce A.: A Fabrication Process for Glass Coated Electron-Bombardment Ion Thruster Grid. NASA TN D-5320, 1969.

Banks, Bruce A.; and Richley, Edward A.: Radially Slotted Grids for a Kaufman Ion Thruster. J. Spacecraft Rockets, vol. 4, no. 11, Nov. 1967, pp. 1562-1563.

Bechtel, Robert T.: Discharge Chamber Optimization of the SERT II Thruster. J. Spacecraft Rockets, vol. 5, no. 7, July 1968, pp. 795-800.

Bechtel, Robert T.: Performance and Control of a 30-Centimeter Diameter, Low Impulse Kaufman Thruster. Paper 69-238, AIAA, Mar. 1969.

Bechtel, R. T.; Csiky, G. A.; and Byers, D. C.: Performance of a 15-Centimeter Diameter, Hollow-Cathode Kaufman Thrustor. Paper 68-88, AIAA, Jan. 1968.

Bogart, Carl D.; and Richley, Edward A.: Space-Charge-Flow Computer Program. NASA TN D-3394, 1966.

Bowditch, David N.: Investigation of the Discharge and Exhaust Beam of a Small Arc Plasma Thrustor. Paper 66-195, AIAA, Mar. 1966.

Bowditch, David N.: A Langmuir Calorimetric Probe to Determine Average Energy Per Ion in a Tenuous Plasma Beam. AIAA J., vol. 5, no. 2, Feb. 1967, pp. 362-363.

Brown, Dennis W.: Some Requirements of Electric and Chemical Thrust Systems for Space Station Drag Cancellation. NASA TN D-1835, 1964.

Brown, Dennis W.: Low-Thrust Orbit Raising in Continuous Sunlight. NASA TN D-2072, 1964.

Burkhart, James A.: Segmented Anode, CO_2-H_2 Performance and Hollow Cathode Erosion Tests on a Low Power MPD Arc Thruster. Paper 69-242, AIAA, Mar. 1969.

Byers, David C.: Performance of Various Oxide-Magazine Cathodes in Kaufman Thrusters. NASA TN D-5074, 1969.

Byers, David C.: Effect of Power Supply Impedance on the SERT II Neutralizer. NASA TM X-52543, 1969.

Byers, David C.: An Experimental Investigation of a High-Voltage Electron-Bombardment Ion Thruster. J. Electrochem. Soc., vol. 116, no. 1, Jan. 1969, pp. 9-17.

Byers, David C.; Kerslake, William R.; and Grobman, Jack: Experimental Investigation of Heavy-Molecule Propellants in an Electron-Bombardment Thrustor. NASA TN D-2401, 1964.

Byers, David C.; and Staggs, John F.: SERT II Flight-Type Thruster System Performance. Paper 69-235, AIAA, Mar. 1969.

Childs, J. H.: Design of Ion Rockets and Test Facilities. Paper 59-103, Inst. Aeron. Sci., June 1959.

Childs, J. Howard: Theoretical Performance of Reverse-Feed Cesium Ion Engines. NASA TN D-876, 1961.

Childs, J. Howard; and Cybulski, Ronald J.: SERT and Early Electric Propulsion Systems. Astron. Aerospace Eng., vol. 1, no. 4, May 1963, pp. 112-117.

Childs, J. Howard; and Mickelsen, William R.: Grid Electrode Ion Rockets for Low Specific Impulse Missions. Presented at Second AFOSR Symposium on Advanced Propulsion Concepts, Boston, Mass., Oct. 7-8, 1959.

Chubb, Donald L.: Ionizing Shock Structure in a Monatomic Gas. Rep. 34, Columbia Univ., Mar. 1967. (Available from DDC as AD-663211.)

Chubb, Donald L.; and Seikel, George R.: Basic Studies of a Low Density Hall Current Ion Accelerator. NASA TN D-3250, 1966. Also Paper 66-76, AIAA, Jan. 1966.

Cohen, Allan J.: A Numerical Analysis of Direct Nuclear Electrogenerator Cells that Use Cerium 144 Beta-Emitting Radioisotope Sources. NASA TN D-2070, 1963.

Cohen, Allan J.: Onset of Anomalous Diffusion in Electron-Bombardment Ion Thrustor. NASA TN D-3731, 1966.

Cohen, Allan J.: Anomalous Diffusion in a Plasma Formed from the Exhaust Beam of an Electron-Bombardment Ion Thruster. NASA TN D-4758, 1968.

Cohen, Allan J.: An Electron-Bombardment Thruster Operated with a Cusped Magnetic Field. NASA TN D-5448, 1969.

Cohen, Allan J.; and Koral, Kenneth F.: Backscattering and Secondary-Electron Emission from Metal Targets of Various Thicknesses. NASA TN D-2782, 1965.

Cohen, Allan J.; and Low, Charles A., Jr.: A Parametric Study of Direct Nuclear Electrogenerator Cells Using a Beta Emitting Source. Paper 63048-B, AIAA, Mar. 1963.

Cook, Harlan; and Richley, Edward A.: Measurements of Efflux Patterns and Flow Rates from Cylindrical Tubes in Free-Molecule and Slip Flows. NASA TN D-2480, 1964.

Cooper, Dale W.; and Kuhns, Perry W.: Measurement of Ion and Electron Densities of Electron-Bombardment Ion-Thrustor Beam. NASA TN D-3761, 1966.

Connolly, Denis J.: Radiation from Sources Immersed in a Partly Ionized Gas. Rep. A-41, Case Inst. Tech. (NASA CR-94598), 1968.

Connolly, D. J.; and Sovie, R. J.: The Effect of Background Pressure and Magnetic Field Shape on MPD Thruster Performance. Paper 69-243, AIAA, Mar. 1969.

Connolly, Denis J.; Sovie, Ronald J.; Michels, Charles J.; and Burkhart, James A.: Low Environmental Pressure MPD Arc Tests. AIAA J., vol. 6, no. 7, July 1968, pp. 1271-1276.

Connolly, Denis J.; and Tanenbaum, B. Samuel: Radiation from Current Sources in an Isotropic Plasma. J. Appl. Phys., vol. 38, no. 6, May 1967, pp. 2557-2562.

Csiky, George A.: Measurements of Some Properties of a Discharge from a Hollow Cathode. NASA TN D-4966, 1969.

Csiky, George A.: Investigation of a Hollow Cathode Discharge Plasma. Paper 69-258, AIAA, Mar. 1969.

Cybulski, R. J.; and Kotnik, J. T.: Evaluation of a Cesium-Ion Rocket Employing a Large Porous Tungsten Ionizer. AIAA J., vol. 1, no. 6, June 1963, pp. 1293-1297.

Cybulski, Ronald J.; Kotnik, Joseph T.; and Lockwood, David L.: Experimental Performance of an Ion Rocket Engine Using A Rectangular-Slab Porous-Tungsten Emitter. NASA TN D-1321, 1962.

Cybulski, Ronald J.; and Lockwood, David L.: An Experimental Evaluation of Two-Dimensional Ion Engine with Charge Neutralization. Paper 61-82-1776, Inst. Aeron. Sci., June 1961.

Cybulski, Ronald J.; Richley, Edward A.; and Keller, Thomas A.: Application of Liquid-Helium Cryopumping to Large Electric Rocket Vacuum Facilities. 1961 Vacuum Symposium Transactions. Vol. 2. Luther E. Preuss, ed., Macmillan Co., 1962, pp. 1279-1284.

Dangle, E. E.; and Lockwood, D. L.: NASA Experimental Research with Ion Rockets. Paper 1126-60, ARS, May 1960.

Domitz, Stanley: Experimental Evaluation of a Direct-Current Low-Pressure Plasma Source. NASA TN D-1659, 1963.

Domitz, Stanley; and Pawlik, Eugene V.: Beam Current Measuring Device for Ion Engine Research. AIAA J., vol. 1, no. 3, Mar. 1963, pp. 712-713.

Dugan, John V., Jr.; and Rice, James H.: A Computer Plotting Description of Ion-Molecule Collisions with Long-Lived Capture Complexes. NASA TN D-5407, 1969.

Dugan, John V., Jr.; and Sovie, Ronald J.: Volume Ion Production Costs in Tenuous Plasmas: A General Atom Theory and Detailed Results for Helium, Argon, and Cesium. NASA TN D-4150, 1967.

Evvard, J. C.: Electric Space Propulsion. Electrical Eng., vol. 79, no. 7, July 1960, pp. 555-563.

Evvard, John C.: A Viewpoint on Space Propulsion and Power-Generation Systems. Proceedings of Fourth International Symposium on Space Technology and Science. Tamiya Nomura, ed., Japan Publications Trading Co., 1963, pp. 417-426.

Evvard, John C.: How Much Future for Electric Propulsion? Astron. Aerospace Eng., vol. 1, no. 7, Aug. 1963, pp. 92-97.

Evvard, John C.: Perspective on Aerospace Propulsion Systems. Ann. N. Y. Acad. Sci., vol. 134, Nov. 22, 1965, pp. 342-354.

Evvard, John C.: Renewed Optimism in Electric Propulsion. Astron. Aeron., vol. 4, no. 2, Feb. 1966, pp. 77-78.

Finke, Robert C.: A Study of Parameters Affecting the Maximum Voltage Capabilities of Shielded Negative Dielectric Junction Vacuum Insulators. Presented at the Second International Symposium on Insulation of High Voltages in Vacuum, Cambridge, Mass., Sept. 7-9, 1966.

Finke, Robert C.; Holmes, Arthur D.; and Keller, Thomas A.: Space Environment Facility for Electric Propulsion Systems Research. NASA TN D-2774, 1965.

Friedlander, Alan L.: Analysis of Guidance Perturbations for a Low-Thrust Mars Orbiter Mission Using SNAP-8. NASA TN D-1433, 1962.

Gold, Harold: A Spacecraft for Ion Thrustor Flight Tests. Paper 865B, SAE, Apr. 1964.

Goldin, Daniel S.: A Thermodynamic Flow Analysis of Particle Formation Efficiency in a Mixed Flow Colloid Thrustor. Paper 67-85, AIAA, Jan. 1967.

Goldin, Daniel S.; and Kvitek, George L.: An Analysis of Particle Formation Efficiency in a Colloid Thrustor. Paper 66-253, AIAA, Mar. 1966.

Goldin, Daniel S.; and Norgren, Carl T.: Thrust Measurements of Colloidal Particles as an Indication of Particle Size and Thrustor Operation. Paper 63050, AIAA, Mar. 1963.

Hamza, Vladimir: Numerical Solution of Axially Symmetric Poisson Equation; Theory and Application to Ion-Thrustor Analysis. NASA TN D-1711, 1963.

Hamza, Vladimir; and Richley, Edward A.: Numerical Solution of Two-Dimensional Poisson Equation: Theory and Application to Electrostatic-Ion-Engine Analysis. NASA TN D-1323, 1962.

Hamza, Vladimir; and Richley, Edward A.: Numerical Evaluation of Ion-Thrustor Optics. NASA TN D-1665, 1963.

Headley, Larry C.: Status of Porous Ionizers for Contact Ionization of Cesium. NASA TN D-3997, 1967.

Hrach, Frank J.: Out-Of-The-Ecliptic-Plane Probe Mission Employing Electric Propulsion. NASA TN D-4455, 1968.

Johansen, A. E.; Bowditch, D. N.; and Burkhart, J. A.: Experimental Performance of a Low-Power MPD Arc Thrustor. Paper 67-50, AIAA, Jan. 1967.

Johansen, Albert E.; and Palmer, Raymond W.: Lightweight Magnets for MPD Arcs. Paper 67-686, AIAA, Sept. 1967.

Jones, Robert E.: Results of Large Vacuum Facility Tests of an MPD Arc Thruster. AIAA J., vol. 4, no. 8, Aug. 1966, pp. 1455-1456.

Jones, Robert E.; and Palmer, Raymond W.: Traveling Wave Plasma Engine Program at NASA Lewis Research Center. Proceedings of the 3rd Symposium on Engineering Aspects of Magnetohydrodynamics. Norman W. Mather and George W. Sutton, eds., Gordon and Breach Science Publ., 1964, pp. 383-399.

Jones, Robert E.; and Palmer, Raymond W.: Experimental Investigation of a Constant-Velocity Traveling Magnetic Wave Plasma Engine. NASA TN D-2676, 1965.

Kaufman, Harold R.: One-Dimensional Analysis of Ion Rockets. NASA TN D-261, 1960.

Kaufman, Harold R.: The Neutralization of Ion-Rocket Beams. NASA TN D-1055, 1961.

Kaufman, Harold R.: An Ion Rocket with an Electron-Bombardment Ion Source. NASA TN D-585, 1961.

Kaufman, Harold R.: Electron Diffusion in a Turbulent Plasma. NASA TN D-1324, 1962.

Kaufman, Harold R.: The Electron-Bombardment Ion Rocket. Advanced Propulsion Concepts. Vol. 1. Gordon and Breach Science Publ., 1963, pp. 3-17.

Kaufman, Harold R.: Performance Correlation for Electron-Bombardment Ion Sources. NASA TN D-3041, 1965.

Kaufman, Harold R.; and Reader, Paul D.: Experimental Performance of Ion Rockets Employing Electron-Bombardment Ion Sources. Paper 1374-60, ARS, Nov. 1960.

Keller, Thomas A.: NASA Electric Rocket Test Facilities. 1960 Vacuum Symposium Transactions. C. Robert Meissner, ed., Pergamon Press, 1961, pp. 161-167. Also presented at Symposium on Rocket Operations at Simulated High Altitudes and in Space, Tullahoma, Tenn., June 28-29, 1961.

Kemp, Robert F.; Sellen, J. M., Jr.; and Pawlik, Eugene V.: Beam Neutralization Tests of a Flight Model Electron Bombardment Engine. Paper 2663-62, ARS, Nov. 1962.

Kemp, Robert F.; Sellen, J. M., Jr.; and Pawlik, Eugene V.: Neutralizer Tests on a Flight-Model Electron-Bombardment Thrustor. NASA TN D-1733, 1963.

Kerrisk, D. J.; and Kaufman, H. R.: Electric Propulsion Systems for Primary Spacecraft Propulsion. Paper 67-424, AIAA, July 1967.

Kerslake, William R.: Accelerator Grid Tests on an Electron-Bombardment Ion Rocket. NASA TN D-1168, 1962.

Kerslake, William R.: Charge-Exchange Effects on the Accelerator Impingement of an Electron-Bombardment Ion Rocket. NASA TN D-1657, 1963.

Kerslake, William R.: Cathode Durability in the Mercury Electron-Bombardment Ion Thrustor. Paper 64-683, AIAA, Aug. 1964.

Kerslake, William R.: Preliminary Operation of Oxide-Coated Brush Cathodes in Electron-Bombardment Ion Thrustors. NASA TM X-1105, 1965.

Kerslake, William R.: Oxide-Cathode Durability in the Mercury Electron-Bombardment Ion Engine. NASA TN D-3818, 1967.

Kerslake, William R.; Byers, David C.; and Staggs, John F.: SERT II Experimental Thrustor System. Paper 67-700, AIAA, Sept. 1967.

Kerslake, William R.; Margosian, Paul M.; and Wasserbauer, Joseph F.: Experimental Mercury Bombardment Thruster at Sub-Millipound Test. AIAA J., vol. 5, no. 4, Apr. 1967, pp. 683-691.

Kerslake, William R.; and Pawlik, Eugene V.: Additional Studies of Screen and Accelerator Grids for Electron-Bombardment Ion Thrustors. NASA TN D-1411, 1963.

Koral, Kenneth F.: Prebreakdown Currents, High Voltage Conditioning and Ultimate Voltage for a Large-Gap Concentric Cylinder Configuration in Vacuum. Presented at the Second International Symposium on Insulation of High Voltages in Vacuum, Cambridge, Mass., Sept. 7-9, 1966.

Koral, Kenneth F.: High-Voltage Characteristics of a Large-Gap Coaxial-Cylinder Electrode. NASA TN D-3949, 1967.

Koral, Kenneth F.; and Cohen, Allan J.: Empirical Equations for Electron Back Scattering Coefficients. NASA TN D-2909, 1965.

Kotnik, J. Thomas: Evaluation of a Hollow, Cylindrical, Contact-Ion Source. NASA TN D-1187, 1962.

Kotnik, J. Thomas; and Sater, Bernard L.: Power-Conditioning Requirements for Ion Rockets. IEEE Trans. on Aerospace, vol. AS-2, Apr. 1964, pp. 496-504.

Lathem, Walter C.: Effects of Electrode Misalinements in Kaufman Thrusters. J. Spacecraft Rockets, vol. 5, no. 6, June 1968, pp. 735-737.

Lathem, Walter C.: A New Technique for Simulating Space-Charge Potential Distributions. J. Spacecraft Rockets, vol. 5, no. 6, June 1968, pp. 737-738.

Lathem, Walter C.: Ion Accelerator Designs for Kaufman Thrusters. Paper 69-261, AIAA, Mar. 1969.

Lathem, Walter C.; and Staggs, John F.: Divergent-Flow Contact-Ionization Electrostatic Thrustor for Satellite Attitude Control and Station Keeping. NASA TN D-4420, 1968.

Lockwood, David L.; and Cybulski, Ronald J.: Performance Evaluation of a Two-Dimensional Ion Rocket Using Through-Feed and Porous Tungsten Ionizers. NASA TN D-766, 1961.

Lockwood, David L.; and Hamza, Vladimir: Space-Charge-Flow Theory and Electrode Design for Electrostatic Rocket Engines. NASA TN D-1461, 1962.

Lockwood, David L.; Mickelsen, William R.; and Hamza, Vladimir: Analytic Space-Charge Flow and Theoretical Electrostatic Rocket Engine Performance. Paper 2400-62, ARS, Mar. 1962.

Low, Charles A., Jr.: Radioisotope Heating for Contact Ionization Thrustors. Paper 67-735, AIAA, Sept. 1967.

Low, Charles A., Jr.; and Mickelsen, William R.: A Radioisotope Electrostatic Propulsion System. Trans. Am. Nucl. Soc., vol. 5, no. 2, Nov. 1962, p. 429.

Low, Charles A., Jr.; and Mickelsen, William R.: An Electrostatic Propulsion System with a Direct Nuclear Electrogenerator. Aerospace Eng., vol. 21, no. 12, Dec. 1962, pp. 58-59, 72-87.

MacKay, John S.; and Rossa, Leonard G.: A Variational Method for the Optimization of Interplanetary Round-Trip Trajectories. NASA TN D-1660, 1963.

MacKay, John S.; Zola, Charles L.; Rossa, Leonard G.; Fishbach, Laurence H.; Strack, William C.; and Hrach, Frank J.: Manned Mars Landing Missions Using Electric Propulsion. NASA TN D-3194, 1966.

Margosian, Paul M.: Parametric Study of a Thermoelectrostatic Generator For Space Applications. NASA TN D-2763, 1965.

Margosian, Paul M.: Preliminary Tests of Insulated Accelerator Grid for Electron-Bombardment Thrustor. NASA TM X-1342, 1967.

Margosian, Paul M.; and Kerslake, William R.: Experimental Evaluation of a Two-Directional Electron-Bombardment Ion Thrustor. AIAA J., vol. 5, no. 5, May 1967, pp. 833-839.

Maslowski, Edward A.: Experimental Data on Pumping of Mercury Ion Beams by Liquid-Nitrogen-Cooled Condensers. NASA TN D-3231, 1966.

Michels, Charles J.: Study of Coaxial Plasma-Gun Exhaust. Bull. Am. Phys. Soc., vol. 8, no. 5, 1963, p. 441.

Michels, Charles J.; and Ramins, Peter: Performance of Coaxial Plasma Gun with Various Propellants. Phys. Fluids, vol. 7, no. 11, pt. 2, Nov. 1964, pp. S71-S74.

Michels, Charles J.: Some Transient Electrical Characteristics of the Exhaust of a Self-Crowbarred Coaxial Plasma Gun. NASA TN D-2571, 1965.

Michels, Charles J.: Coaxial Plasma Gun Research at Lewis Research Center. NASA TM X-1600, 1968.

Michels, Charles J.: A Resume of Research on Coaxial Plasma Guns Performed at Lewis Research Center. Presented at the Seminar on Coaxial Plasma Guns, Catholic Univ. of America, Washington, D. C., May 10, 1968.

Michels, Charles J.: Dynamic Current-Voltage Characteristics of a Nitrogen MPD-Arc Plasma Source. Presented at the Fall Meeting of the Ohio Section of the Am. Phys. Soc., Columbus, Ohio, Oct. 17-18, 1969.

Michels, C. J.; Heighway, J. E.; and Johansen, A. E.: Analytical and Experimental Performance of Capacitor Powered Coaxial Plasma Guns. AIAA J., vol. 4, no. 5, May 1966, pp. 823-830.

Michels, Charles J.; and Hettel, Henry J.: Transient Spectral Study of Discharges in Coaxial Plasma Guns. Proceedings of the American Physical Society Topical Conference on Pulsed-High-Density Plasmas. Rep. LA-3770, Los Alamos Scientific Lab., Sept. 29, 1967, pp. E6-1 to E6-5.

Michels, Charles J.; and Hettel, Henry J.: Correlation of Transient Spectra with Performance in Coaxial Plasma Guns. NASA TN D-4385, 1968.

Michels, Charles J.; and Johansen, Albert E.: Experimental and Theoretical Performance of Coaxial Plasma Guns. NASA TN D-3469, 1966.

Michels, Charles J.; and Terdan, Fred F.: Characteristics of a 5-Kilojoule, Ignitron-Switched, Fast-Capacitor Bank. NASA TN D-2808, 1965.

Mickelsen, William R.: Electric Propulsion for Space Flight. Aerospace Eng., vol. 19, no. 11, Nov. 1960, pp. 6-11, 36-52.

Mickelsen, William R.: Comparative Performance of Electrostatic Rocket Engines. Paper 62-74, Inst. Aerospace Sci., Jan. 1962.

Mickelsen, William R.: Theoretical Performance of Electrostatic Thrustors with Analytic Space-Charge Flows. NASA TR R-174, 1963.

Mickelsen, William R.: NASA Research on Heavy-Particle Electrostatic Thrustors. Paper 63-19, Inst. Aerospace Sci., Jan. 1963.

Mickelsen, William R.: Electric Propulsion. Space/Aeronautics 1964/65 R&D Handbook, vol. 42, no. 4, Sept. 1964, pp. 50-53.

Mickelsen, William R.: Performance Parameters for Electric-Propulsion Systems. J. Spacecraft Rockets, vol. 3, no. 2, Feb. 1966, pp. 213-218.

Mickelsen, William R.; and Childs, J. Howard: Theoretical Analysis of Ultra-high Vacuum Condensers. Rev. Sci. Instr., vol. 29, no. 10, Oct. 1958, pp. 871-873.

Mickelsen, William R.; and Kaufman, Harold R.: Status of Electrostatic Thrustors for Space Propulsion. NASA TN D-2172, 1964.

Mickelsen, William R.; and Kaufman, Harold R.: Electrostatic Thrustors for Space Propulsion, Present and Future. J. Brit. Interplanet. Soc., vol. 19, pt. 8, Apr. 1964, pp. 319-337.

Mickelson, William R.; and Low, Charles A., Jr.: Potentials of Radioisotope Electrostatic Propulsion. Astron. Aerospace Eng., vol. 1, no. 9, Oct. 1963, pp. 52-57.

Mickelson, William R.; and MacKay, John S.: Interplanetary Flight with Electric Propulsion. Astron. Aeron., vol. 3, no. 1, Jan. 1965, pp. 44-49.

Milder, Nelson L.: Fragmentation of Anthracene in an Electron-Bombardment Ion Source. NASA TN D-2592, 1965.

Milder, Nelson L.: A Survey and Evaluation of Research on the Discharge Chamber Plasma of a Kaufman Thruster. Paper 69-494, AIAA, June 1969.

Milder, Nelson L.; and Kaufman, Harold R.: Analysis of Electron Analog Simulation of Ion Containment in Magnetic Fields. NASA TN D-5217, 1969.

Milder, Nelson L.; and Kerslake, William R.: Evaluation of Filament Deterioration in Electron-Bombardment Ion Sources. NASA TN D-2173, 1964.

Mirels, Harold: Two-Dimensional Ion Beams with Small Lateral Spreading. NASA TN D-679, 1961.

Mirels, Harold; and Rosenbaum, Burt M.: Analysis of One-Dimensional Ion Rocket With Grid Neutralization. NASA TN D-266, 1960.

Moeckel, W. E.: Trajectories with Constant Tangential Thrust in Central Gravitational Fields. NASA TR R-53, 1959.

Moeckel, W. E.: Propulsion Methods in Astronautics. Advances in Aeronautical Sciences. Vol. 2. Pergamon Press, 1959, pp. 1078-1097.

Moeckel, W. E.: Fast Interplanetary Missions with Low-Thrust Propulsion Systems. NASA TR R-79, 1960.

Moeckel, Wolfgang E.; et al.: Satellite and Space Propulsion Systems. NASA TN D-285, 1960.

Moeckel, W. E.: Status of Electric Propulsion Systems for Space Missions. Advances in Cryogenic Engineering. Vol. 6. K. D. Timmerhaus, ed., Plenum Press, 1961, pp. 3-19.

Moeckel, W. E.: Electric Propulsion Systems for Mars Missions. Exploration of Mars. Vol. 15 of Advances in the Astronautical Sciences. George W. Morgenthaler, ed., Western Periodicals Co., 1963, pp. 79-103.

Moeckel, W. E.: Promises and Potentialities of Electric Propulsion-Status of Thrustor Performance. Paper 66-1024, AIAA, Nov. 1966.

Moeckel, W. E.: Electric Propulsion. Science, vol. 142, Oct. 11, 1963, pp. 172-178.

Nakanishi, Shigeo: Experimental Investigation of a High-Voltage Isolation Device for Ion-Thrustor Propellant Feed. NASA TN D-3535, 1966.

Nakanishi, Shigeo: Experimental Investigation of Mercury Propellant Feed Isolators for Kaufman Thrusters. NASA TM X-1579, 1968.

Nakanishi, S.; Banks, B. A.; and Richley, E. A.: High-Perveance Accelerator Grids for Low-Voltage Kaufman Thrusters. J. Spacecraft Rockets, vol. 5, no. 3, Mar. 1968, pp. 356-358.

Nakanishi, S.; and Pawlik, E. V.: Experimental Investigation of a 1.5-M-Diam Kaufman Thruster. J. Spacecraft Rockets, vol. 5, no. 7, July 1968, pp. 801-807.

Nakanishi, Shigeo; Pawlik, Eugene V.; and Baur, Charles W.: Experimental Evaluation of Steady-State Control Properties of an Electron-Bombardment Ion Thrustor. NASA TN D-2171, 1964.

Nichols, Lester D.: Comparison of Brayton and Rankine Cycle Magnetogas-dynamic Space-Power Generation Systems. NASA TN D-5085, 1969.

Nichols, Lester D.; and Mantenieks, Maris A.: Analytical and Experimental Studies of MHD Generator Cathodes Emitting in a "Spot" Mode. Presented at the ASME Winter Annual Meeting, Los Angeles, Calif., Nov. 16-21, 1969.

Nieberding, William C.; and Lovell, Robert R.: Thrust Measurement of Sert I Ion Thrustors. NASA TN D-3407, 1966.

Norgren, Carl T.: Onboard Colloidal Particle Generator for Electrostatic Engines. Electric Propulsion Development. Vol. 9 of Progress in Astronautics and Aeronautics. Ernst Stuhlinger, ed., Academic Press, 1963, pp. 407-434.

Norgren, Carl T.; and Goldin, Daniel S.: Experimental Analysis of the Exhaust Beam from a Colloid Thrustor. AIAA J., vol. 3, no. 10, Oct. 1965, pp. 1943-1945.

Norgren, Carl T.; Goldin, Daniel S.; and Connolly, Denis J.: Colloid Thrustor Beam Analysis: Design and Operation of a Suitable Quadrupole Mass Filter. NASA TN D-3036, 1965.

Palmer, Raymond W.; and Jones, Robert E.: Experimental Investigation of a Variable-Length Constant-Velocity Traveling Magnetic Wave Plasma Accelerator. NASA TN D-4205, 1967.

Palmer, Raymond W.; Jones, Robert E.; and Seikel, George, R.: Analytical Investigations of Coil-System Design Parameters for a Constant-Velocity Traveling Magnetic Wave Plasma Engine. NASA TN D-2278, 1964.

Pawlik, Eugene V.: An Experimental Evaluation of Array of Three Electron-Bombardment Ion Thrustors. NASA TN D-2597, 1965.

Pawlik, Eugene V.; Margosian, Paul M.; and Staggs, John F.: A Technique for Obtaining Plasma-Sheath Configurations and Ion Optics for an Electron-Bombardment Ion Thrustor. NASA TN D-2804, 1965.

Pawlik, Eugene V.; and Nakanishi, Shigeo: Experimental Evaluation of Size Effects on Steady-State Control Properties of Electron-Bombardment Ion Thrustor. NASA TN D-2470, 1964.

Pawlik, Eugene V.; Nakanishi, Shigeo; and Algeri, Harvey R.: Some Dynamic Characteristics of an Electron-Bombardment Ion Thrustor. NASA TN D-4204, 1967.

Pawlik, Eugene V.; and Reader, Paul D.: Accelerator Grid Durability Tests of Mercury Electron-Bombardment Ion Thrustors. NASA TN D-4054, 1967.

Pawlik, Eugene V.; and Wenger, Norman C.: Performance Evaluation of a Mercury-Propellant Feed System for a Flight-Model Ion Engine. NASA TN D-1213, 1962.

Ramler, James R.: Low-Thrust Orbit Raising in Continuous Sunlight While Thrusting in a Plane Perpendicular to the Earth-Sun Line. NASA TN D-4104, 1967.

Rawlin, Vincent K.; and Kerslake, William R.: Durability of the SERT II Hollow Cathode and Future Applications of Hollow Cathodes. Paper 69-304, AIAA, Mar. 1969.

Rawlin, V. K.; and Pawlik, E. V.: A Mercury Plasma-Bridge Neutralizer. J. Spacecraft Rockets, vol. 5, no. 7, July 1968, pp. 814-820.

Reader, Paul D.: Investigation of a 10-Centimeter-Diameter Electron-Bombardment Ion Rocket. NASA TN D-1163, 1962.

Reader, Paul D.: Scale Effects on Ion Rocket Performance. ARS. J., vol. 32, no. 5, May 1962, pp. 711-714.

Reader, Paul D.: Ion Rocket with a Permanent Magnet. Astron. Aerospace Eng., vol. 1, no. 9, Oct. 1963, p. 83.

Reader, Paul D.: The Operation of an Electron-Bombardment Ion Source with Various Gases. Presented at the International Conference on Electron and Ion Beam Science and Technology, Electrochem. Soc. and the Am. Inst. Mech. Eng., Toronto, Canada, May 5-7, 1964.

Reader, Paul D.: Experimental Performance of a 50 Centimeter Diameter Electron-Bombardment Ion Rocket. Paper 64-689, AIAA, Aug. 1964.

Reader, Paul D.: Experimental Effects of Propellant-Introduction Mode on Electron-Bombardment Ion Rocket Performance. NASA TN D-2587, 1965.

Reader, Paul D.: Durability Tests of Mercury Electron-Bombardment Ion Thrustors. Paper 66-231, AIAA, Mar. 1966.

Reader, Paul D.; and Finke, Robert C.: An Electron-Bombardment Ion Rocket Operated with Alternating-Current Supplies. NASA TN D-1457, 1962.

Reader, P. D.; and King, H. J.: Systems Characteristics of Liquid Mercury Cathode Thrusters. Paper 69-237, AIAA, Mar. 1969.

Reader, Paul D.; and Mickelsen, William R.: Ion Propulsion Systems for Spacecraft. J. Spacecraft Rockets, vol. 2, no. 4, July-Aug. 1965, pp. 577-583.

Reader, Paul D.; and Pawlik, Eugene V.: Cathode Durability Tests in Mercury Electron-Bombardment Ion Thrustors. NASA TN D-4055, 1967.

Reader, Paul D.; and Regetz, John D., Jr.: A Delta Boosted, Electrically Raised Direct Broadcast Synchronous Satellite. Paper 69-1104, AIAA, Oct. 1969.

Reshotko, Eli: Resonance in a Cold Multiconstituent Plasma at Arbitrary Orientation to the Magnetic Field. NASA TN D-1875, 1963.

Reynolds, Thaine W.: Estimation of Critical Temperature for Surface Ion Currents from Electron Emission Data. NASA TN D-1307, 1962.

Reynolds, Thaine W.; and Childs, J. Howard: A Graphical Method for Estimating Ion-Rocket Performance. NASA TN D-466, 1960.

Reynolds, Thaine W.; and Childs, J. Howard: A Comparison of Reverse-Feed and Porous-Tungsten Ion Engines. NASA TN D-1166, 1962.

Reynolds, Thaine W.; and Kreps, Lawrence W.: Gas Flow, Emittance, and Ion Current Capabilities of Porous Tungsten. NASA TN D-871, 1961.

Reynolds, Thaine W.; and Richley, Edward A.: Thermionic Emission from Cesium-Coated Electrostatic Ion-Thrustor Electrodes. NASA TN D-1879, 1963.

Reynolds, Thaine W.; and Richley, Edward A.: Flux Patterns Resulting From Free-Molecule Flow Through Converging and Diverging Slots. NASA TN D-1864, 1964.

Reynolds, Thaine W.; and Richley, Edward A.: Analysis of Free-Molecule Flow with Surface Diffusion Through Cylindrical Tubes. NASA TN D-3225, 1966.

Reynolds, Thaine W.; and Richley, Edward A.: Free-Molecule Flow and Surface Diffusion Through Slots and Tubes - A Summary. NASA TR R-255, 1967.

Reynolds, Thaine W.; and Richley, Edward A.: Propellant Condensation on Surfaces Near An Electric Rocket Exhaust. Paper 69-270, AIAA, Mar. 1969.

Richley, Edward A.: NASA Electrostatic-Thrustor Research and Instrumentation. Presented at Ohio State University Seminar on Experimental Techniques in High-Speed Aerodynamics and Gas Dynamics, Columbus, Ohio, July 8-24, 1963.

Richley, Edward A.; and Bogart, Carl D.: Numerical Solutions of Knudsen Flow Entering a Circular Tube through a Small Axial Orifice. NASA TN D-2115, 1964.

Richley, Edward A.; and Cybulski, Ronald J.: High-Vacuum Condenser Design: Experimental Effects from Cesium and Mercury Ion Beams. NASA TN D-1217, 1962.

Richley, Edward A.; Cybulski, Ronald J.; and Keller, Thomas A.: Experimental Evaluation of High-Vacuum Condensers in Large Vacuum Facilities. 1961 Vacuum Symposium Transactions. Vol. 2. Luther E. Preuss, ed., Macmillan Co., 1962, pp. 1285-1291.

Richley, Edward A.; and Kerslake, William R.: Bombardment Thruster Investigations at the Lewis Research Center. Paper 68-542, AIAA, June 1968.

Richley, Edward A.; and Mickelsen, William R.: Effects of Molecular Flow in Plasma Generation and Some Analyses of Space Charge Flow in Ion Acceleration. Paper 64-7, AIAA, Jan. 1964.

Richley, Edward A.; and Reynolds, Thaine W.: Numerical Solutions of Free-Molecule Flow in Converging and Diverging Tubes and Slots. NASA TN D-2330, 1964.

Richley, E. A.; Sandborn, V. A.; Baldwin, L. V.; and Dangle, E. E.: Comparative Measurements of Beam Power in Ion-Rocket Research. NASA TN D-845, 1961.

Rossa, Leonard G.: A Parametric Study of Constant Thrust, Electrically Propelled Mars and Venus Orbiting Probes. NASA TN D-2154, 1964.

Saunders, Neal T.: Experimental Method of Producing Porous Tungsten for Ion Rocket Engines. NASA TN D-864, 1961.

Schertler, Ronald J.: Outgassing Characteristics of an Epoxy-Impregnated Magnet Coil. NASA TM X-1813, 1969.

Schertler, Ronald J.; and Norgren, Carl T.: Experimental Investigation of Charging Submicron Carbon Powder for Colloidal Particle Thrustors. NASA TN D-3657, 1966.

Schwirian, Richard E.: A New Momentum Integral Method for Treating Magnetohydrodynamic and Simple Hydrodynamic Entrance Flows. NASA TN D-5215, 1969. Also Paper 69-724, AIAA, June 1969.

Seikel, George R.: Generation of Thrust-Electromagnetic Thrustors. Electric Propulsion for Spacecraft. NASA SP-22, 1962, pp. 19-24.

Seikel, George R.: Plasma. Space/Aeronautics, vol. 43, no. 4, Apr. 1965, pp. 40-45.

Seikel, George R.; Bowditch, David N.; and Domitz, Stanley: Application of Magnetic-Expansion Plasma Thrustors to Satellite Station Keeping and Attitude Control Missions. Paper 64-677, AIAA, Aug. 1964.

Seikel, George R.; and Chubb, Donald L.: Simulation of Solar-Wing Magnetosphere Interactions. Bull. Am. Phys. Soc., vol. 13, no. 7, July 1968, p. 959.

Seikel, G. R.; and Reshotko, E.: Hall Current Ion Accelerator. Bull. Am. Phys. Soc., vol. 7, no. 6, June 19, 1962, p. 414.

Shattuck, Russell D.; and Denington, Robert J.: Status and Future Engineering Problems of Electric Propulsion Systems. 2nd Manned Space Flight Meeting, AIAA, 1963, pp. 341-350.

Smith, J. Marlin: Electrothermal Instabilities in the Entrance Region of an MHD Generator. Bull. Am. Phys. Soc., vol. 13, no. 11, Nov. 1968, p. 1564.

Smith, J. Marlin: Electrothermal Instability - An Explanation of the MPD Arc Thruster Rotating Spoke Phenomenon. Paper 69-231, AIAA, Mar. 1969.

Smith, John R.: Self-Consistent Many-Electron Theory of Electron Work Functions and Surface Potential Characteristics for Selected Metals. Phys. Rev., vol. 181, no. 2, May 10, 1969, pp. 522-529.

Sovie, Ronald J.: Volume Ion-Production Efficiency and Spectroscopic Diagnostics in a Helium Plasma. Bull. Am. Phys. Soc., vol. 8, no. 5, 1963, p. 424.

Sovie, Ronald J.: Spectroscopic Determination of Electron Temperature and Percentage Ionization in a Helium Plasma. Phys. Fluids, vol. 7, no. 4, Apr. 1964, pp. 613-614.

Sovie, R. J.: The Effects of Cascading and Metastable Atoms on the Determination of Electron Temperature from Relative Line Intensities in a Tenuous Helium Plasma. J. Quant. Spectrosc. Radiat. Transfer, vol. 8, no. 2, Feb. 1968, pp. 833-838.

Sovie, R. J.: The Effect of Optical Thickness on Spectroscopic Diagnostics and Volume Ion Production in Tenuous Helium Plasmas. Bull. Am. Phys. Soc., vol. 14, no. 2, Feb. 1969, p. 257.

Sovie, R. J.; and Connolly, D. J.: Doppler Measurements of the Exhaust Velocities in an MPD Thruster. Bull. Am. Phys. Soc., vol. 13, no. 11, Nov. 1968, p. 1513.

Sovie, R. J.; and Connolly, D. J.: A Study of the Axial Velocities in an Ammonia MPD Thruster. AIAA J., vol. 7, no. 4, Apr. 1969, pp. 723-725.

Sovie, R. J.; and Dugan, J. V., Jr.: Energy Required for Ion Production by Electron Bombardment in Helium, Argon, and Cesium. Bull. Am. Phys. Soc., vol. 10, no. 2, 1965, p. 179.

Sovie, Ronald J.; and Dugan, John V., Jr.: Effects of Metastable Atoms on Volume Ion Production in a Tenuous Helium Plasma. NASA TN D-3121, 1965.

Sovie, R. J.; and Dugan, J. V., Jr.: Volume Ion Production Costs in Tenuous Plasmas. Bull. Am. Phys. Soc., vol. 12, no. 2, Feb. 1967, p. 239.

Sovie, Ronald J.; and Klein, Barry M.: Volume Ion Production in a Tenuous Helium Plasma. NASA TN D-2324, 1964.

Sovie, R. J.; and Seikel, G. R.: rf Induction Heating and Production of Plasmas. Bull. Am. Phys. Soc., vol. 8, no. 2, 1963, p. 153.

Sovie, Ronald J.; and Seikel, George R.: Radio-Frequency Induction Heating of Low-Pressure Plasma. NASA TN D-4206, 1967. See also Bull. Am. Phys. Soc., vol. 12, no. 5, 1967, p. 813; and Paper 67-732, AIAA, Sept. 1967.

Staggs, John F.: An Electrolytic Tank Analog for Two-Dimensional Analysis of Electrostatic-Thrustor Optics. NASA TN D-2803, 1965.

Staggs, John F.; Gula, William P.; and Kerslake, William R.: Distribution of Neutral Atoms and Charge-Exchange Ions Downstream of an Ion Thruster. J. Spacecraft Rockets, vol. 5, no. 2, Feb. 1968, pp. 159-164.

Staggs, John F.; and Lathem, Walter C.: Experimental Performance of a Low-Thrust, Divergent-Flow, Contact-Ionization Electrostatic Thruster. J. Spacecraft Rockets, vol. 4, no. 5, May 1967, pp. 610-615.

Staggs, John F.: Richley, Edward A.; and Gula, William P.: Ion Extractor System Design. AIAA J., vol. 5, no. 2, Feb. 1967, pp. 359-360.

Stankiewicz, N.: Feasibility of Applying Field-Ion Emission to Electrostatic Rocket Engines. NASA TN D-1563, 1963.

Stankiewicz, N.: Field Emission Charging of Metallic Colloids. NASA TN D-2078, 1963.

Stankiewicz, Norbert: Limits of Validity of Radiationless Decay of High-Density Plasmas. NASA TN D-3372, 1966.

Stankiewicz, Norbert: Thermodynamic Study of Plasmas Using the Principle of Maximum Entropy. NASA TN D-4621, 1968.

Stankiewicz, N.: The Ellipsoidal Velocity Distribution Function. NASA TN D-5026, 1969.

Stevens, N. J.; and Briehl, D. C.: Thermal Investigation of an Ion Engine Microthrustor. NASA TM X-1473, 1967.

Stover, John B.: Electric Breakdown and Arcing in Experimental Ion Thrustor Systems. Paper 63-057, AIAA, Mar. 1963.

Stover, John B.: Effect of Thrustor Arcing on Ion Rocket System Design. Paper 64-682, AIAA, Aug. 1964.

Strack, William C.: Combined High-Low Thrust Propulsion for the Close Solar Probe Mission. NASA TN D-3145, 1965.

Strack, William C.; and Huff, Vearl N.: The N-Body Code - A General FORTRAN Code for the Numerical Solution of Space Mechanics Problems of an IBM 7090 Computer. NASA TN D-1730, 1963.

Strack, William C.; and Zola, C. L.: Solar-Electric Propulsion Probes for Exploring the Solar System. NASA TM X-52318, 1967.

Walker, E. L.; and Tanenbaum, B. Samuel: Investigation of Kinetic Models for Gas Mixtures. Phys. Fluids, vol. 11, no. 9, Sept. 1968, pp. 1951-1954.

Walker, E. L.; and Tanenbaum, B. Samuel: Transport Equations for a Weakly Ionized Electron Gas. Phys. Fluids, vol. 11, no. 9, Sept. 1968, pp. 1955-1958.

Wasserbauer, Joseph F.: Experimental Performance of a High-Current-Density Cylindrical Concave Porous Tungsten Emitter for Ion Thrustors. Paper 63-029, AIAA, Mar. 1963.

Wasserbauer, Joseph F.: Field-Enhanced Thermionic Emission From Electrodes of Cesium Ion Thrustor. NASA TN D-2635, 1965.

Wasserbauer, Joseph F.: A 5-Centimeter-Diameter Electron-Bombardment Thrustor with Permanent Magnets. NASA TN D-3628, 1966.

Zimmerman, Arthur V.; MacKay, John S.; and Rossa, Leonard G.: Optimum Low-Acceleration Trajectories for Interplanetary Transfers. NASA TN D-1456, 1963.

Zola, Charles L.: Trajectory Methods in Mission Analysis for Low-Thrust Vehicles. Paper 64-51, AIAA, Jan. 1964.

Zola, Charles L.: Jovian Planet Missions for Solar Cell Powered Electric Propulsion Spacecraft. Paper 68-118, AIAA, Jan. 1968.

TABLE I-1. - SUMMARY OF 30-CENTIMETER-DIAMETER THRUSTER PERFORMANCE

Beam power	600 V × 1.5 A	900 W
Discharge power	35 V × 7.5 A (175 eV × 1.5 A)	262 W
Power losses:		165 W
Accelerator	1200 V × 0.07 A	84 W
Vaporizer/feed[a]		13 W
Cathode tip/keeper[a]		13 W
Neutralizer[a]		55 W

[a]Estimate based on current SERT II data.

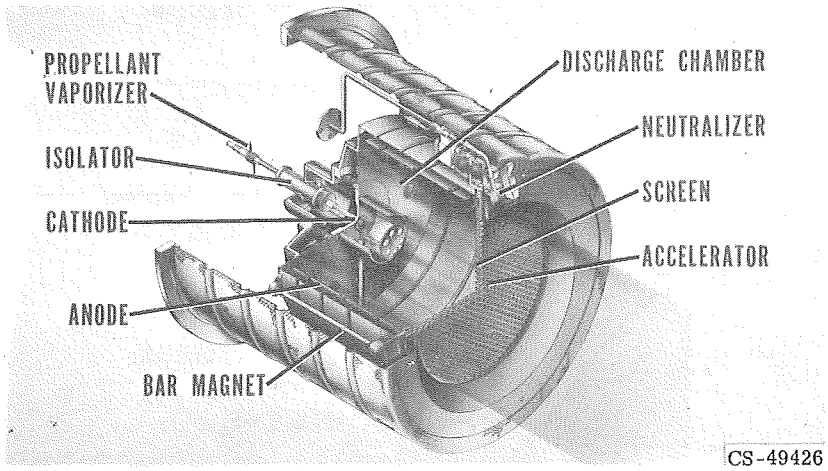

Figure I-1. - Electron-bombardment ion thruster.

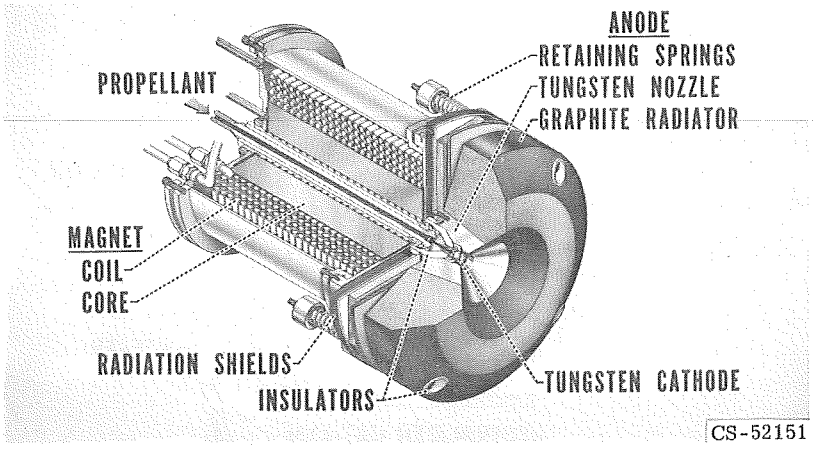

Figure I-2. - 30-Kilowatt MPD arc thruster.

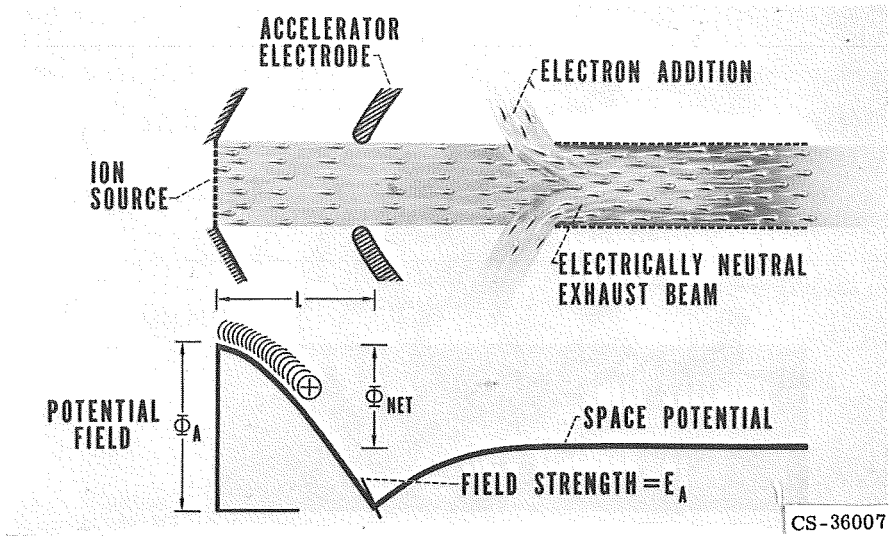

Figure I-3. - Electrostatic acceleration.

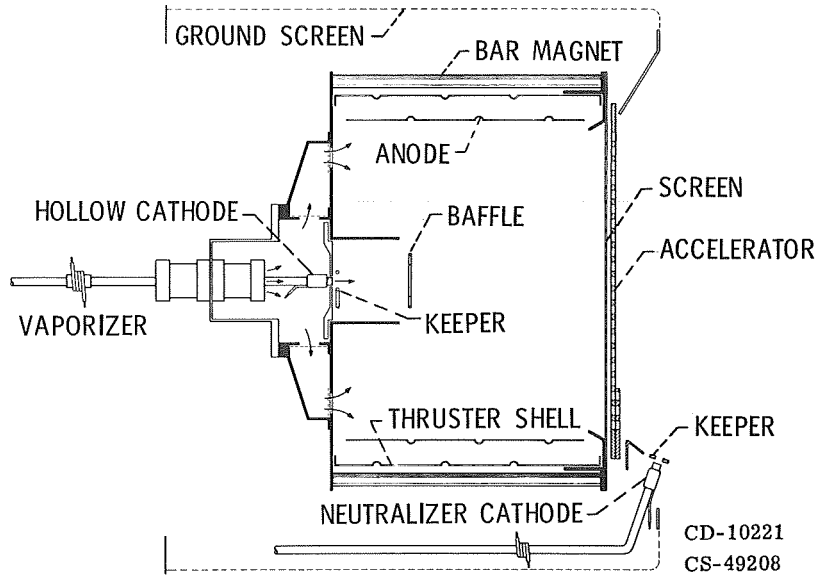

Figure I-4. - 15-Centimeter-diameter experimental SERT II thruster.

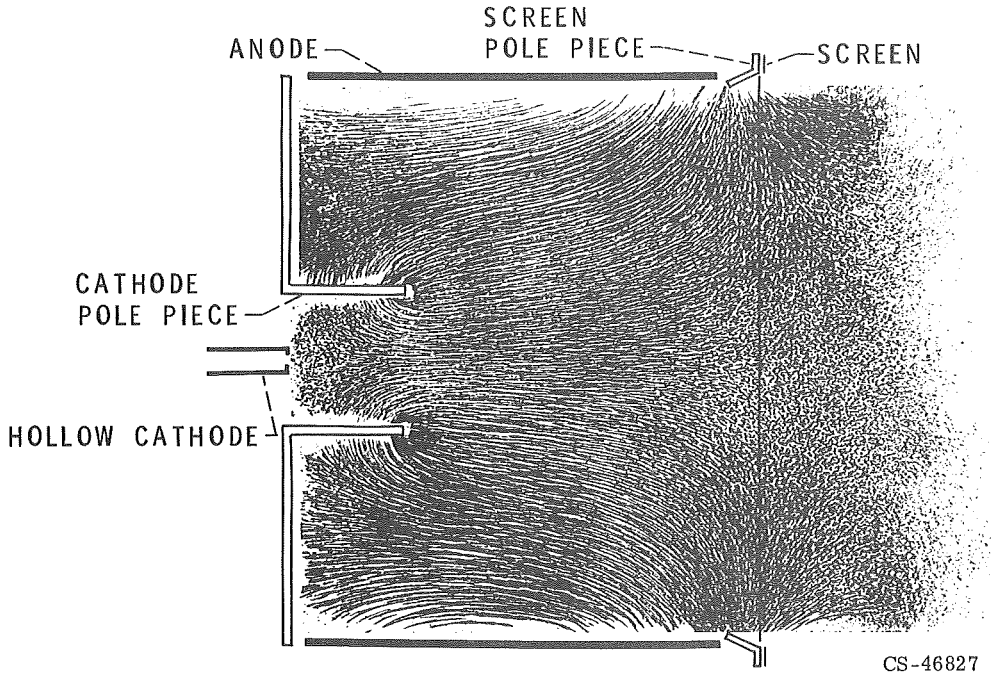

Figure I-5. - SERT II thruster magnetic field map.

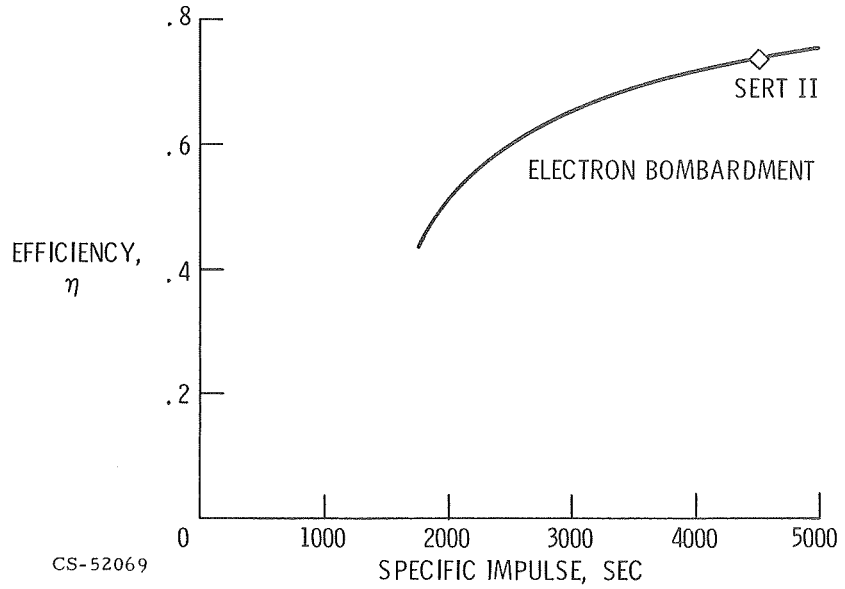

Figure I-6. - Thruster performance.

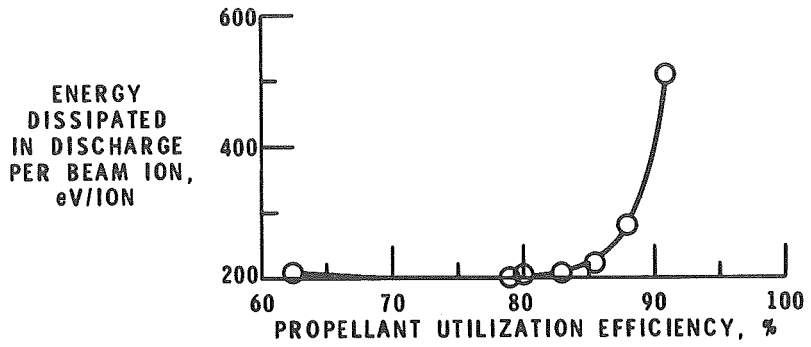

CS-43923

Figure I-7. - Variation of energy dissipated in discharge per beam ion with propellant utilization efficiency.

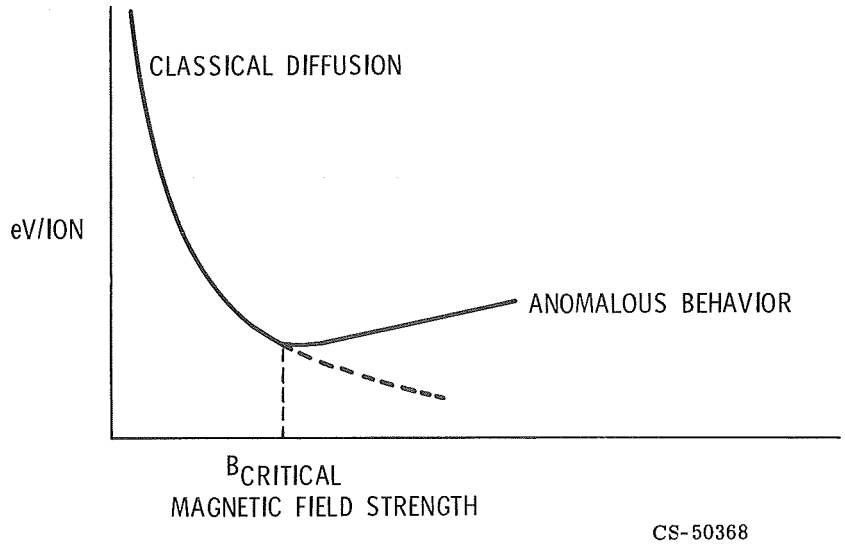

CS-50368

Figure I-8. - Discharge energy loss against magnetic field strength.

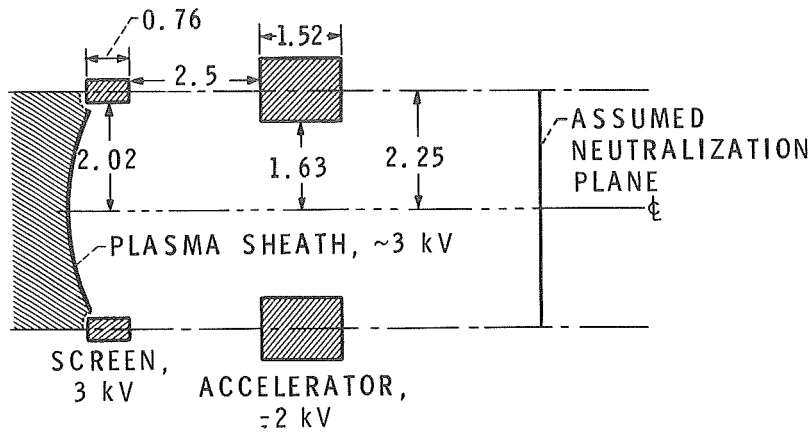

Figure I-9. - Single hole of SERT II grid system. Dimensions are in millimeters.

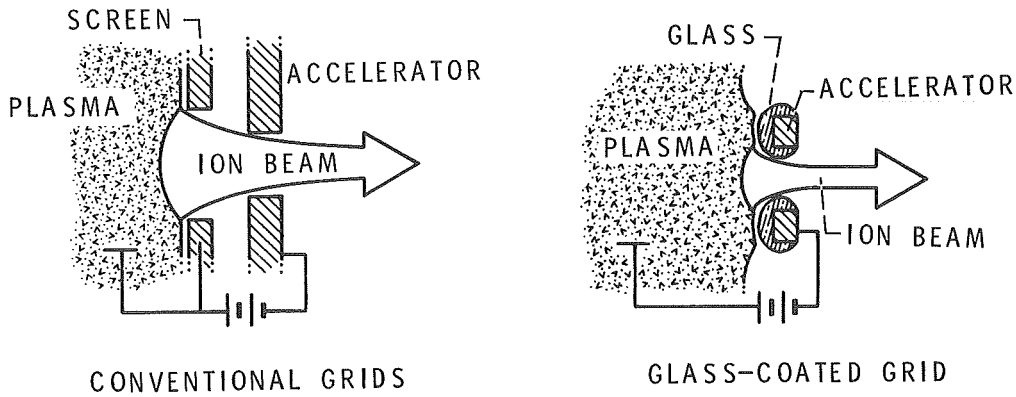

Figure I-10. - Comparison of accelerator grid concepts.

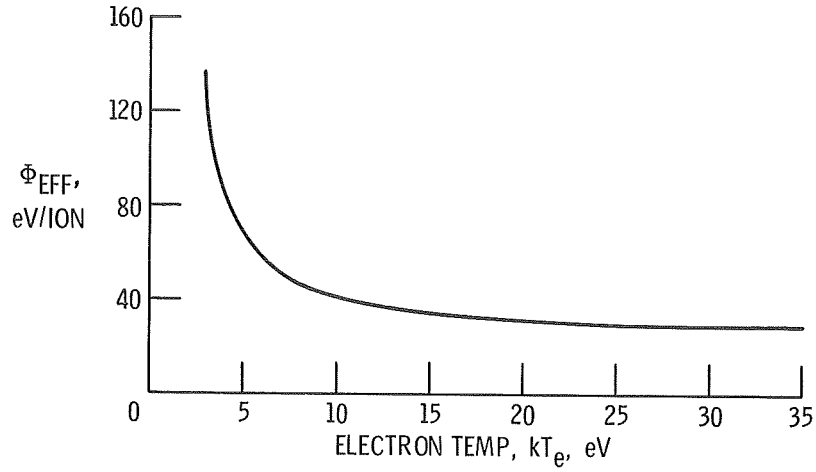

Figure I-11. - Volume ion production cost for mercury.

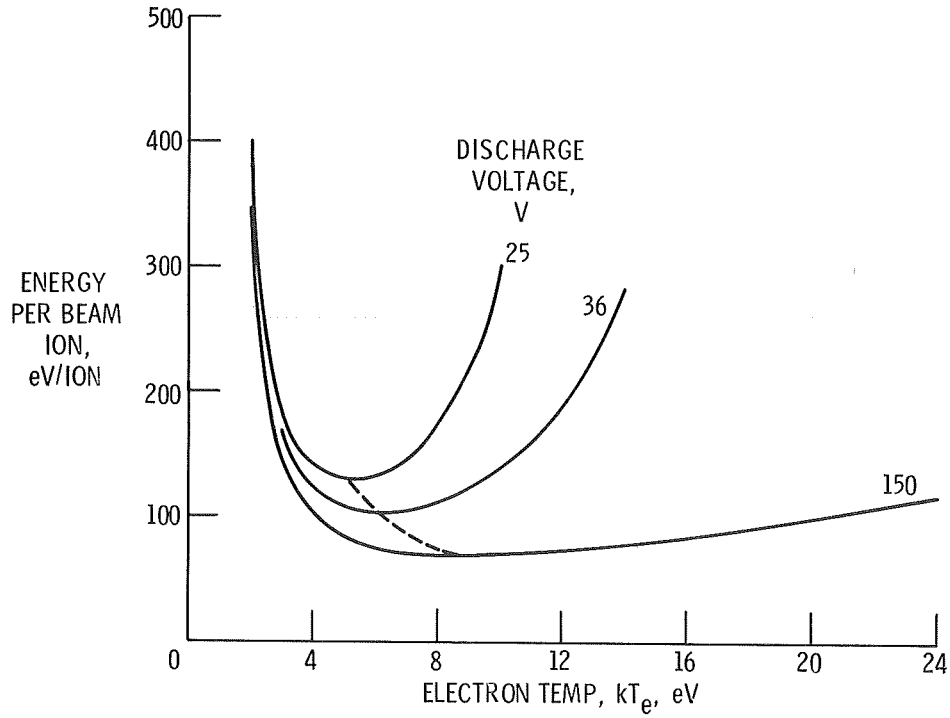

Figure I-12. - Direct current mercury source performance limit. Anode work function, Φ_A = 4.5 volts.

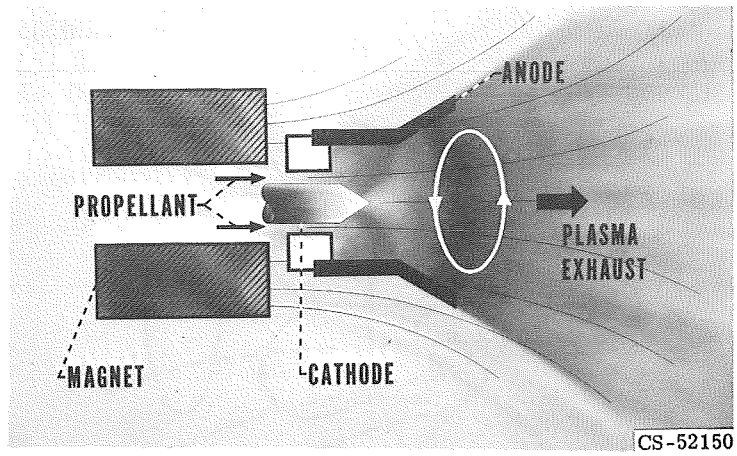

Figure I-13. - MPD arc thruster.

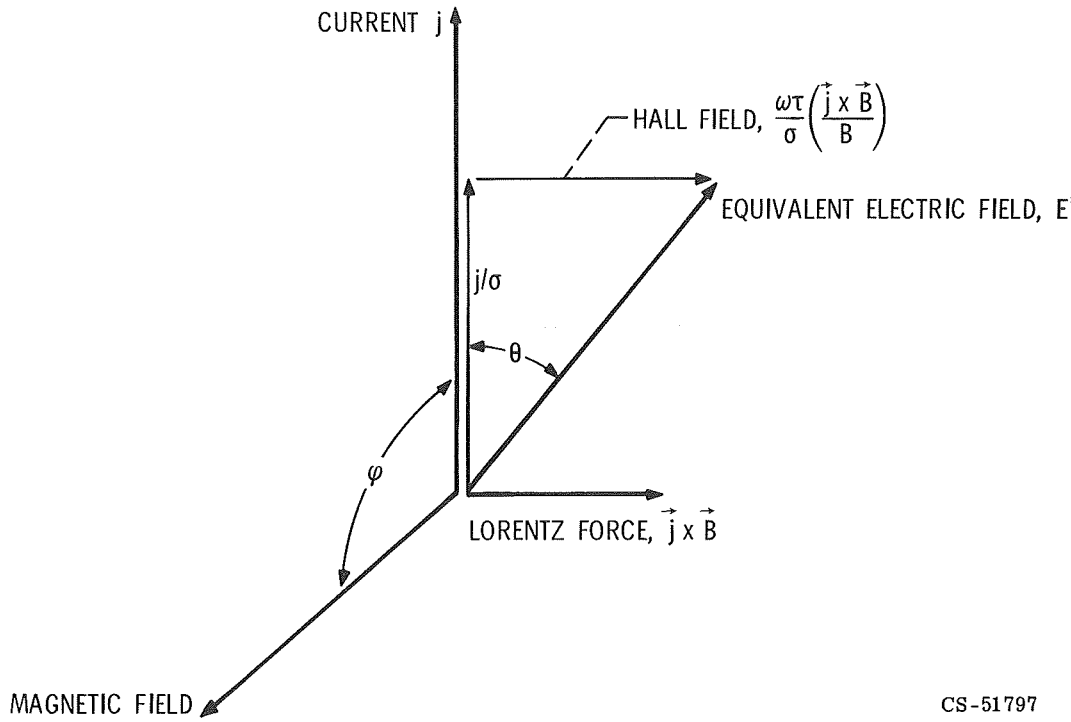

Figure I-14. - Vector diagram of plasma current, magnetic field, and electric field.

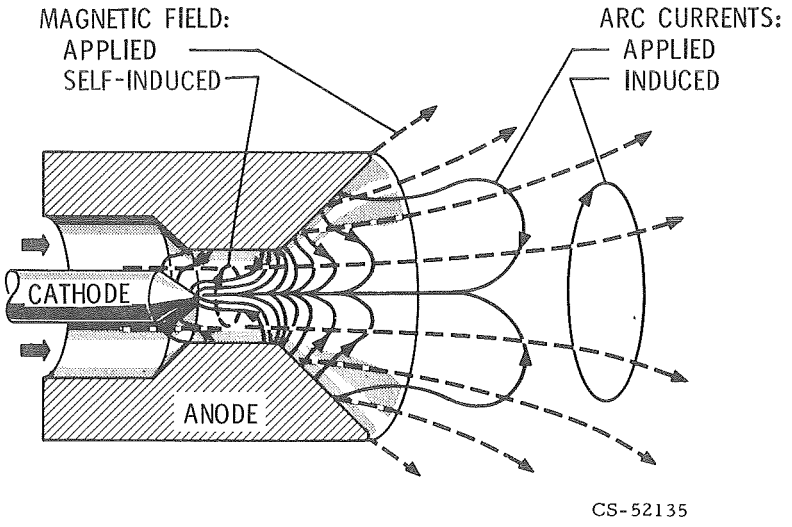

Figure I-15. - MPD arc thruster currents and magnetic fields.

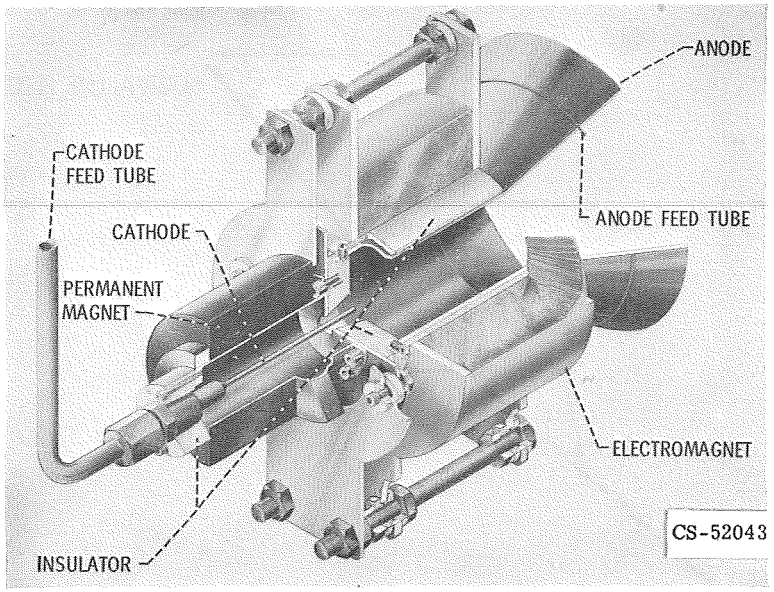

Figure I-16. - 1/2-Kilowatt MPD arc thruster.

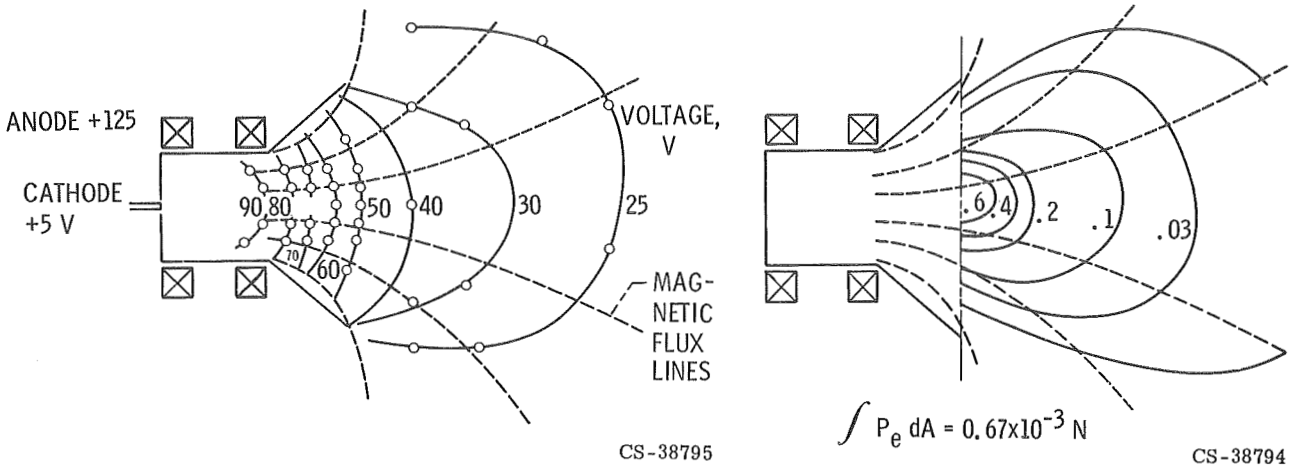

(a) Plasma potential profiles.

(b) Electron gas pressure profiles.

Figure I-17. - Subkilowatt MPD arc thruster.

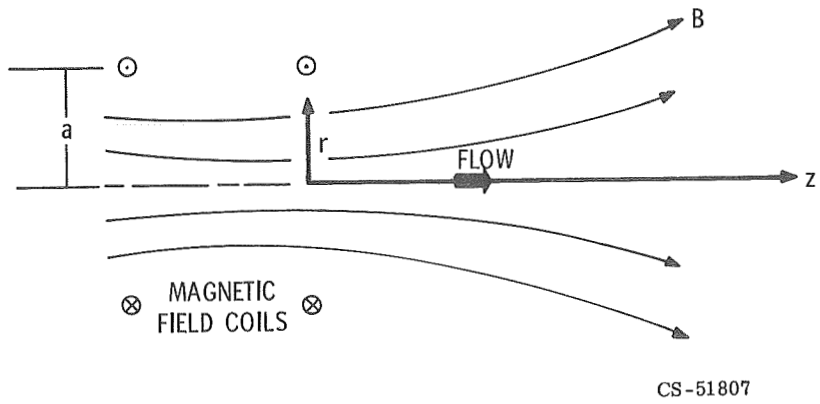

Figure I-18. - Plasma expansion in a magnetic nozzle.

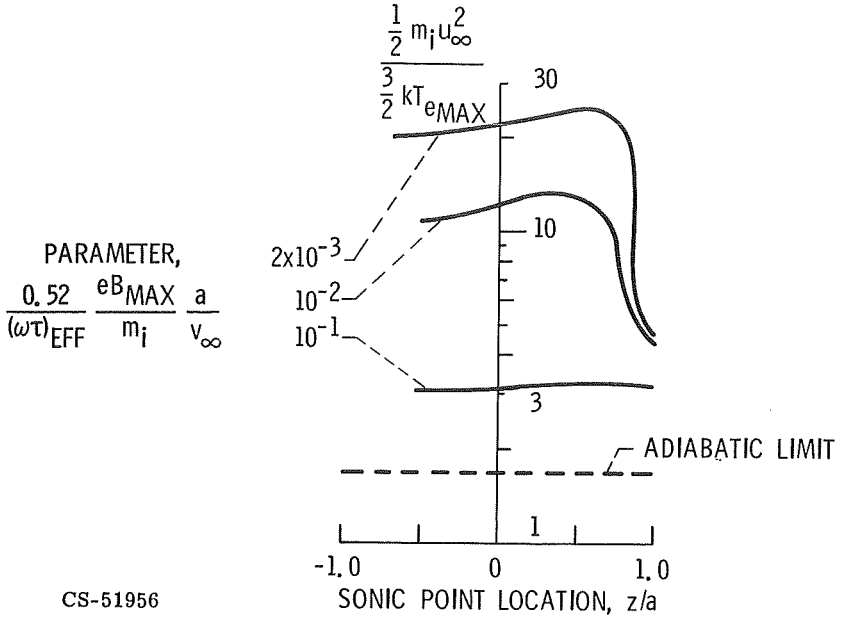

Figure I-19. - Ratio of final ion to initial electron energy as function of sonic point location.

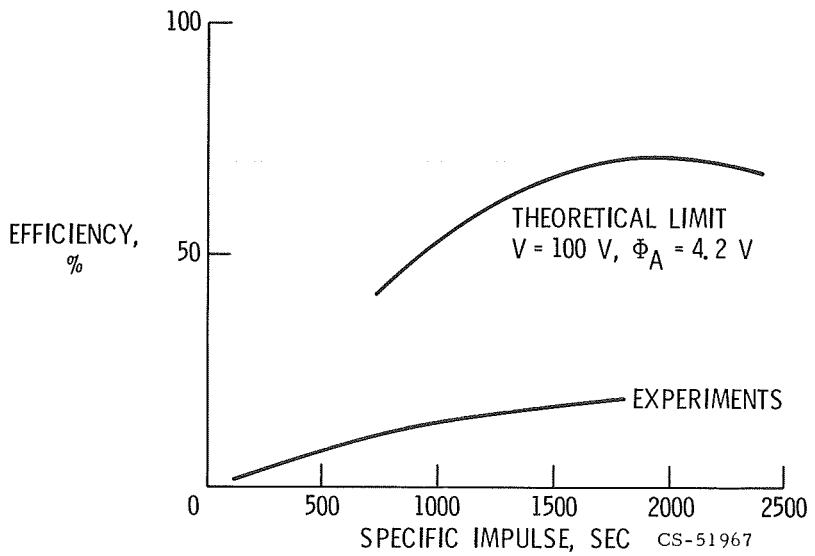

Figure I-20. - Low power xenon MPD arc thruster.

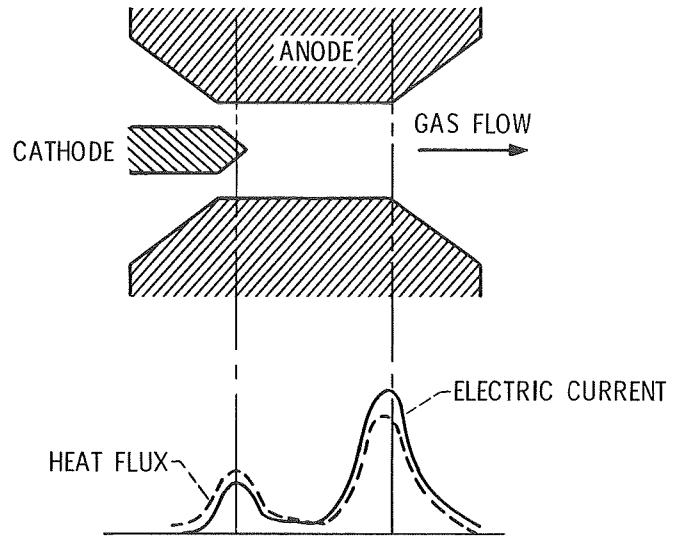

CS-52070

Figure I-21. - Anode current and heat flux distribution.

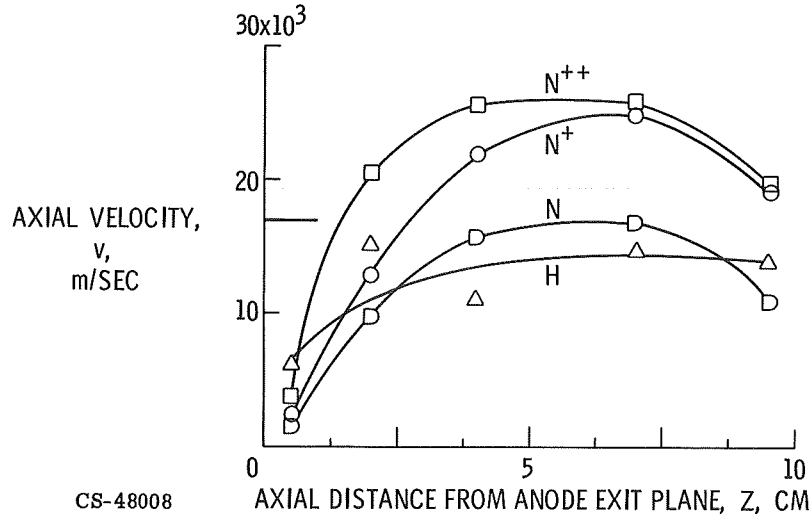

CS-48008

Figure I-22. - Axial velocity as function of axial distance. Specific impulse, 1765 seconds.

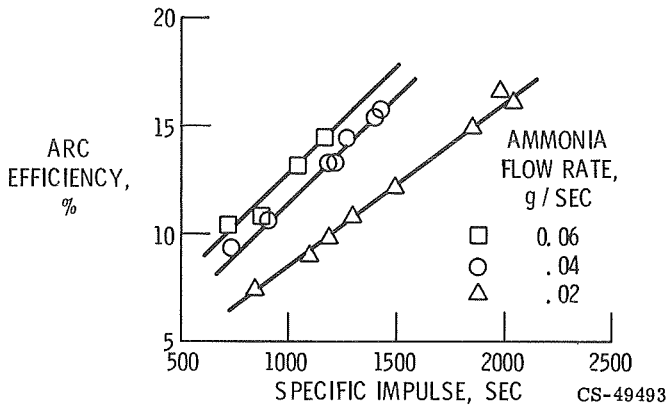

Figure I-23. - Arc efficiency as function of specific impulse.

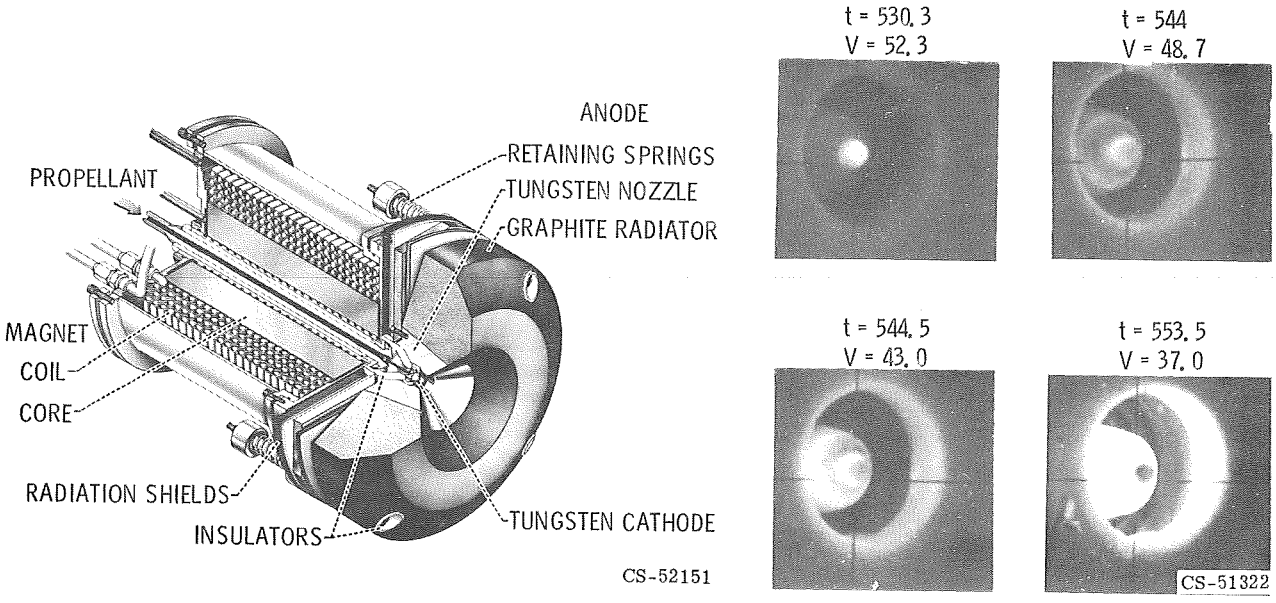

(a) 30-Kilowatt MPD arc thruster.

(b) Progressive change in cathode attachment.

Figure I-24. - Relation between arc voltage and cathode current attachment.

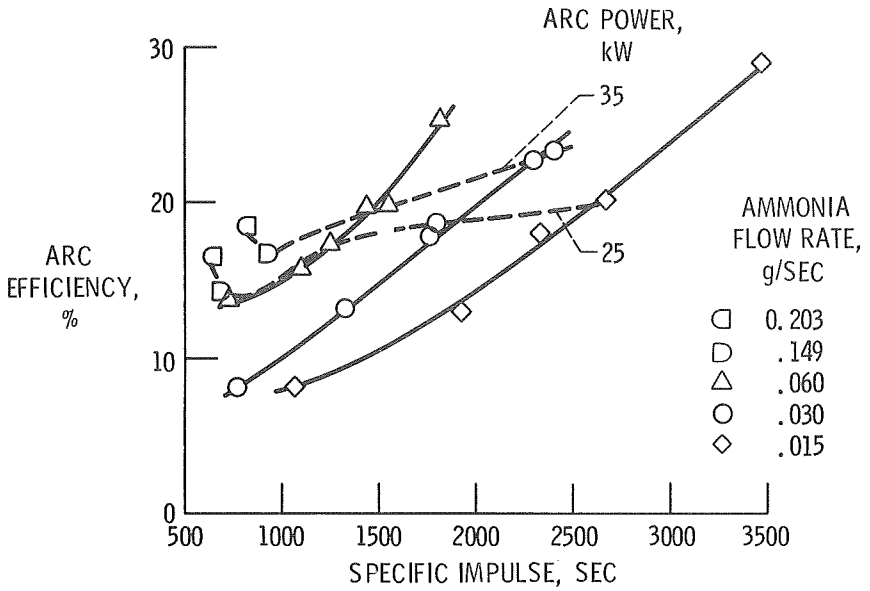

Figure I-25. - 30-Kilowatt thruster efficiency as function of specific impulse.

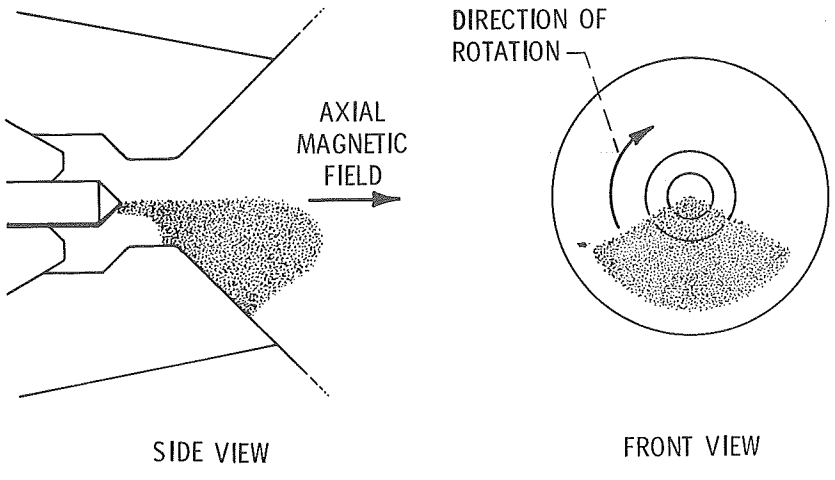

Figure I-26. - Rotating current spoke.

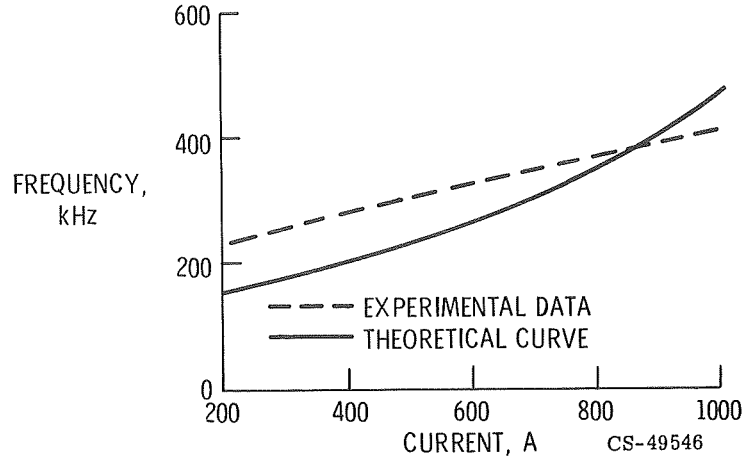

Figure I-27. - Frequency as function of current in ammonia. Mass flow, 0.03 gram per second; magnetic field, 0.100 tesla.

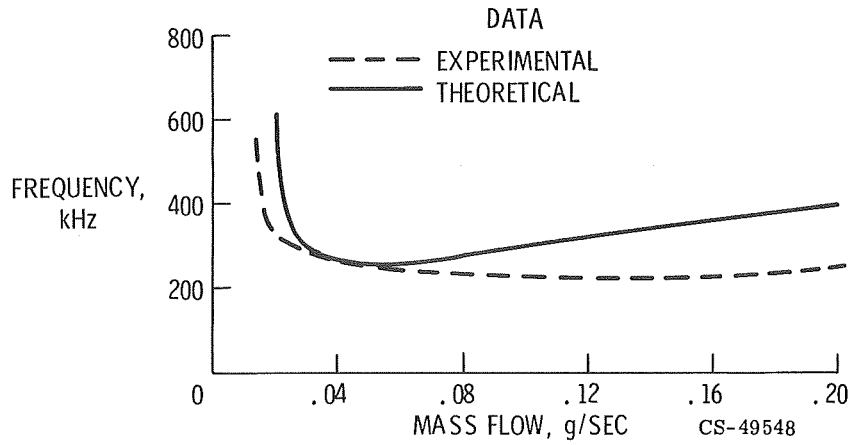

Figure I-28. - Frequency as function of mass flow in ammonia. Current, 600 amperes; magnetic field, 0.125 tesla.

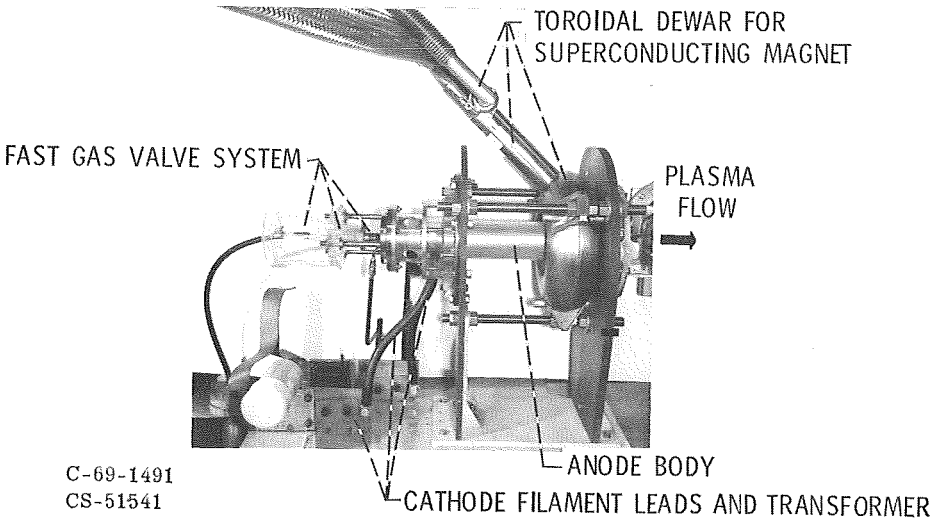

Figure I-29. - Megawatt MPD-arc plasma source.

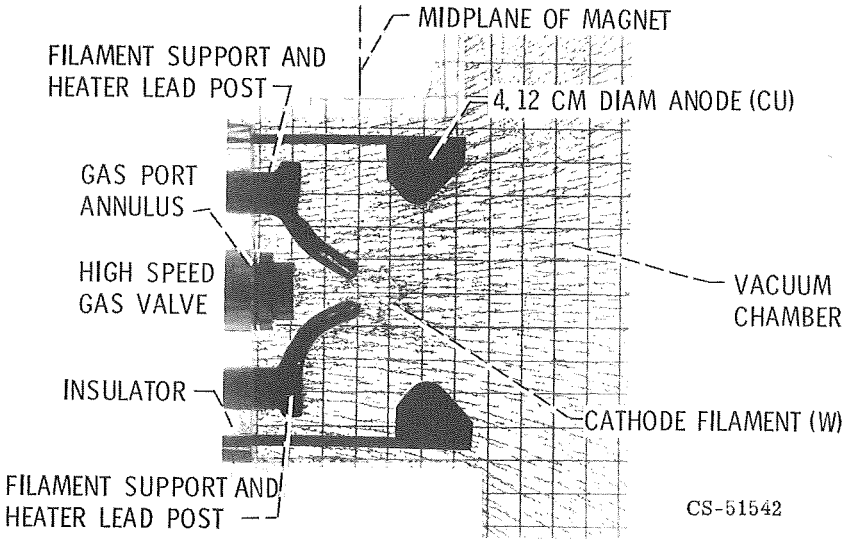

Figure I-30. - Arc chamber.

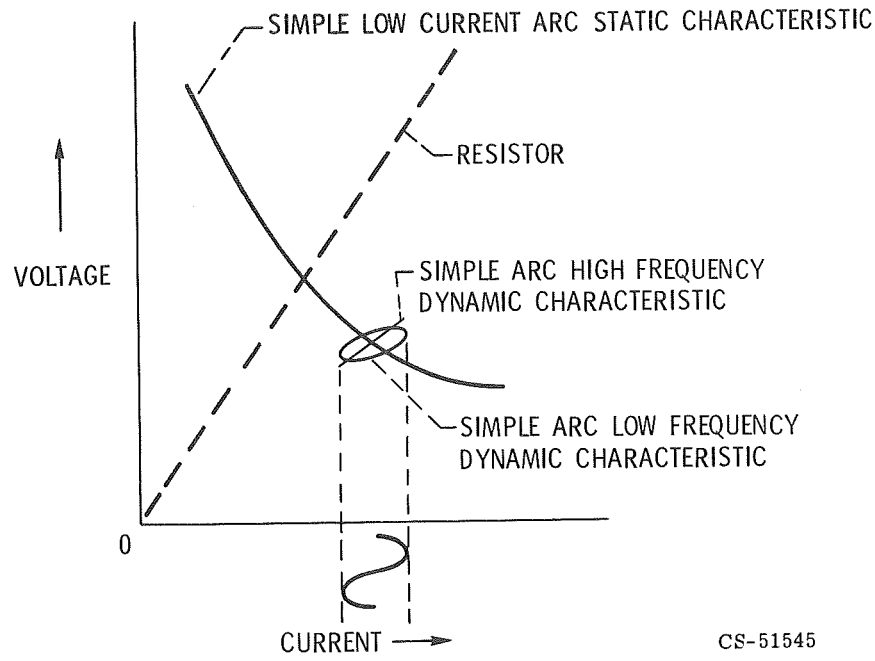

Figure I-31. - General voltage-current characteristic.

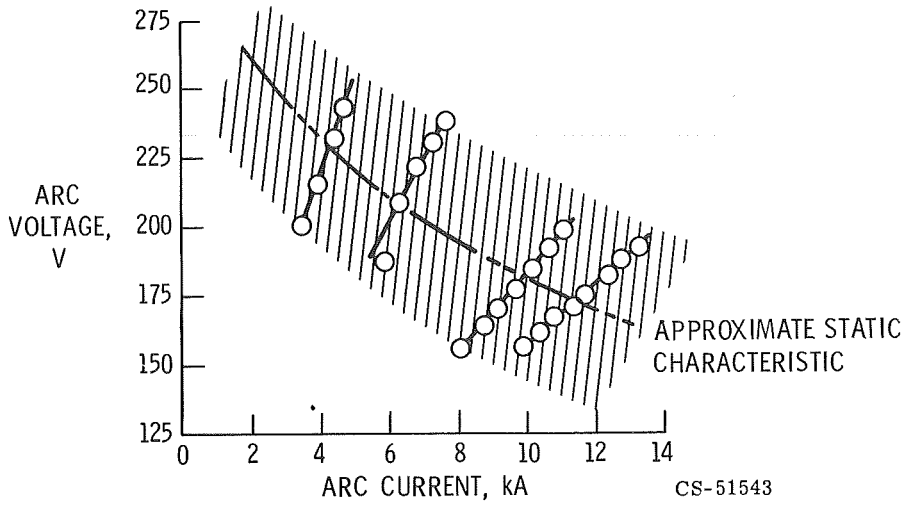

Figure I-32. - Dynamic characteristics of megawatt MPD-arc source. Magnetic field, 0.75 tesla.

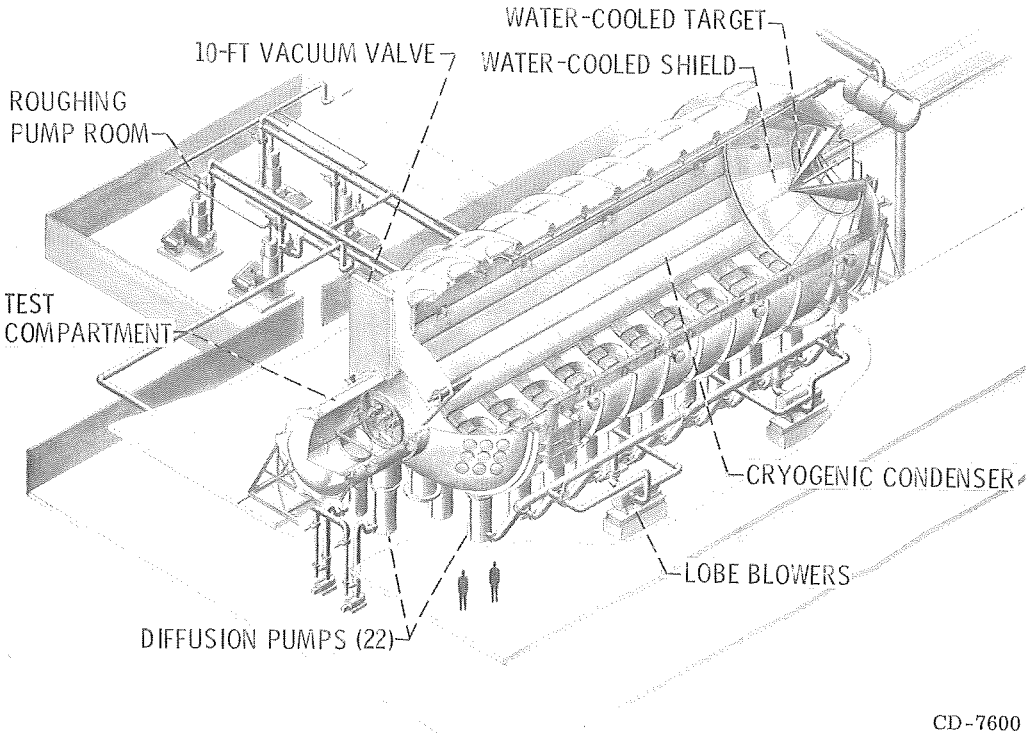

(a) Cutaway view of 25-foot-diameter tank.

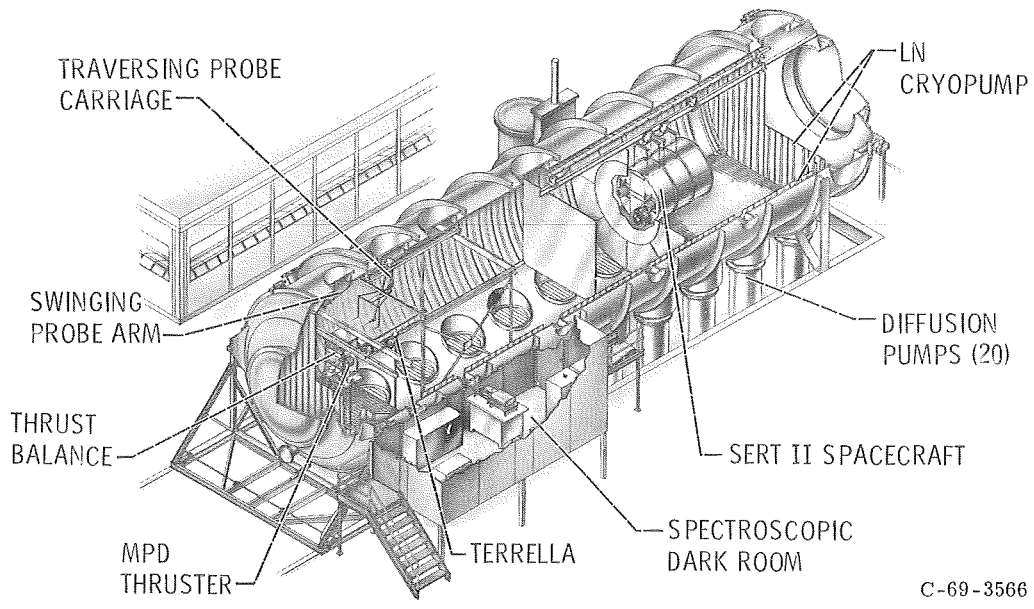

(b) Cutaway view of 15-foot-diameter tank.

Figure I-33. - Electropropulsion test facility.

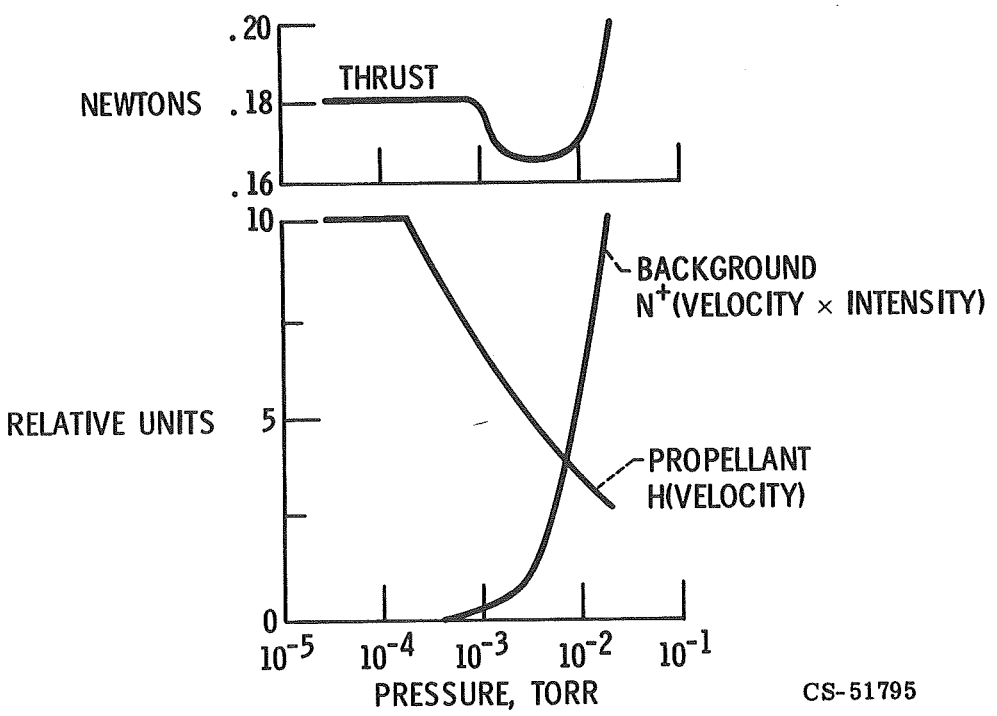

Figure I-34. - Relation between measured thrust and spectroscopic measurements in exhaust.